INVESTIGATION OF SOLID STATE PHASE TRANSFORMATIONS IN MANGANESE-ALUMINUM ALLOYS

A THESIS SUBMITTED TO
THE GRADUATE SCHOOL OF NATURAL AND APPLIED SCIENCES
OF
MIDDLE EAST TECHNICAL UNIVERSITY

BY

ÖZGÜN ACAR

IN PARTIAL FULFILLMENT OF THE REQUIREMENTS
FOR
THE DEGREE OF MASTER OF SCIENCE
IN
METALLURGICAL AND MATERIALS ENGINEERING

SEPTEMBER 2016

Approval of the thesis:

INVESTIGATION OF SOLID STATE PHASE TRANSFORMATIONS IN MANGANESE-ALUMINUM ALLOYS

submitted by **ÖZGÜN ACAR** in partial fulfillment of the requirements for the degree of **Master of Science in Metallurgical and Materials Engineering Department, Middle East Technical University** by,

Prof. Dr. Gülbin Dural Ünver _____
Dean, Graduate School of **Natural and Applied Sciences**

Prof. Dr. C. Hakan Gür _____
Head of Department, **Metallurgical and Materials Engineering**

Assoc. Prof. Dr. Y. Eren Kalay _____
Supervisor, **Metallurgical and Materials Eng. Dept., METU**

Assist. Prof. Dr. İlkay Kalay _____
Co-Supervisor, **Materials Sci. and Eng. Dept., Çankaya Uni.**

Examining Committee Members:

Prof. Dr. C. Hakan Gür _____
Metallurgical and Materials Engineering Dept., METU

Assoc. Prof. Dr. Y. Eren Kalay _____
Metallurgical and Materials Engineering Dept., METU

Assoc. Prof. Dr. Yiğit Karpat _____
Industrial Engineering Dept., Bilkent University

Assist. Prof. Dr. Mert Efe _____
Metallurgical and Materials Engineering Dept., METU

Assist. Prof. Dr. Batur Ercan _____
Metallurgical and Materials Engineering Dept., METU

Date: 09.09.2016

I hereby declare that all information in this document has been obtained and presented in accordance with academic rules and ethical conduct. I also declare that, as required by these rules and conduct, I have fully cited and referenced all material and results that are not original to this work.

Name, Last name: Özgün Acar

Signature :

ABSTRACT

INVESTIGATION OF SOLID STATE PHASE TRANSFORMATIONS IN MANGANESE-ALUMINUM ALLOYS

Acar, Özgün

M.S., Department of Metallurgical and Materials Engineering

Supervisor: Assoc. Prof. Dr. Y. Eren Kalay

Co-Supervisor: Assist. Prof. Dr. İlkay Kalay

September 2016, 84 pages

Permanent magnets have a wide range of application areas such as electric motors, loudspeakers, and generators. The permanent magnet industry is highly dependent on rare-earth (RE) elements. Because of the strategical importance of these RE elements, these magnets become less available and more expensive to reach, which bears a need for RE-free permanent magnets with higher magnetic properties than the conventionally available ones. Mn-Al alloys have a great potential of being used in emerging magnetic applications.

This study mainly focused on the solid-state phase transformations of Mn-Al magnetic alloys. In the first part, general characterization of Mn-Al alloys was conducted. Several characteristics of the system were examined. It was observed that composition had an important effect on the magnetic behavior of the system. Alloys with

manganese content higher than 71.0 wt% contained the stable phases only and they showed paramagnetic behavior. The in-situ heating high-energy X-ray diffraction (HEXRD) was used to understand phase transformations and critical kinetic analyses were conducted. The composition was ineffective on the activation energies and the activation energy of τ phase formation was calculated as ~140 kJ/mol. In the second part, detailed in-situ heating HEXRD experiments were conducted. The dependence of ε to τ phase transformation on ε' phase was investigated. The relationship between the ferromagnetic behavior of the system and composition was observed. It was found that the presence of ε' phase rather than the ε phase acts as the precursor for the ferromagnetic τ phase. The formation of τ phase is designated by the presence of ε' phase.

Keywords: Permanent magnets, Mn-Al alloys, τ-MnAl, ε' phase, ferromagnetic, high-energy X-ray diffraction

ÖZ

MANGAN-ALÜMİNYUM ALAŞIMLARINDAKİ KATI HAL FAZ DÖNÜŞÜMLERİNİN ARAŞTIRILMASI

Acar, Özgün

Yüksel Lisans, Metalurji ve Malzeme Mühendisliği Bölümü

Tez Yöneticisi: Doç. Dr. Y. Eren Kalay

Ortak Tez Yöneticis: Yrd. Doç. Dr. İlkay Kalay

Eylül 2016, 84 sayfa

Kalıcı mıknatısların elektrik motorları, hoparlörler, ve jeneratörler gibi geniş uygulama alanları vardır. Kalıcı mıknatıs endüstrisi büyük ölçüde nadir toprak elementlerine bağlıdır. Bu nadir toprak elementlerinin stratejik öneminden dolayı, bu mıknatıslar daha zor ulaşılır ve daha pahalı hale gelmiştir, ve bu durum, yaygın olarak kullanılanlardan daha yüksek manyetik özelliklere sahip, nadir toprak elementi içermeyen kalıcı mıknatıslar için bir ihtiyaç doğurmuştur. Mn-Al alaşımları, kalıcı mıknatıs uygulamalarında büyük kullanım potansiyeline sahiptir.

Bu çalışma temel olarak Mn-Al manyetik alaşımlarındaki katı hal faz dönüşümlerine odaklanmıştır. İlk kısımda, Mn-Al alaşımlarının genel karakterizasyonu yapılmıştır. Sistemin çeşitli karakteristik özellikleri incelenmiştir. Kompozisyonun sistemin manyetik davranışı üzerinde önemli etkisi olduğu gözlemlenmiştir. Manganez içeriği ağırlıkça %71.0'den fazla olan alaşımlar yalnızca kararlı fazları içeriyordu ve paramanyetik özellik gösterdi. Faz dönüşümlerini anlamak için yerinde ısıtmalı

yüksek enerjili X-ışını kırınımı kullanılmış ve kritik kinetik analizler yapılmıştır. Kompozisyon aktivasyon enerjileri üzerinde etkisizdi ve τ fazı oluşum aktivasyon enerjisi ~140 kJ/mol olarak hesaplandı. İkinci kısımda, detaylı yerinde ısıtmalı yüksek enerjili X-ışını kırınım deneyleri gerçekleştirilmiştir. ε fazından τ fazına dönüşümünün ε' fazına olan bağlılığı araştırılmıştır. Ferromanyetik davranış ve kompozisyon arasındaki ilişki gözlemlenmiştir. ε fazı yerine ε' fazının ferromanyetik τ fazı oluşumunda öncü olduğu bulunmuştur. τ fazının oluşumu ε' fazının varlığıyla belirlenmektedir.

Anahtar Kelimeler: Kalıcı mıktnatıslar, Mn-Al alaşımları, τ-MnAl, ε' fazı, ferromanyetik, yüksek enerjili X-ışını kırınımı

To my dear family,

ACKNOWLEDGEMENTS

The in-situ heating high energy X-ray diffraction experiment in the BL04-MSPD beamline of ALBA Synchrotron facility was supported by Turkish Atomic Energy Authority (TAEK). I would like to acknowledge Oriol Vallcorba for his help and support during the experiments in ALBA. I would also like to acknowledge Bengi Yağmurlu, Mehmet Yıldırım and others who helped a lot during my experiments and supported me through my hard work.

To start with, I would like to thank my advisor Assoc. Prof. Dr. Y. Eren Kalay for his invaluable contributions to my thesis, academic career, and my life. I would also like to express how grateful I am for his patience and support. I am happy that he accepted me for my master degree when I first asked him during my graduation project when I was still an undergraduate. His guidance meant a lot to me and I hope that our relation would never end.

I was happy to know all of my lab mates. I have shared a lot with Mertcan Başkan, my former labmate, who was also my former classmate, is the earliest one that I have met. I am also thankful to Ayşe Merve Ünalan for her support and patience during our studies together. She was always kind to me and very helpful. Besides them, I am very happy and glad to know and build a friendship with Mustafacan Kutsal, Fatih Sıkan, Bengisu Yaşar, Serkan Yılmaz, Mert Övün, Eyüp Can Demir, Gökhan Polat, Ayşe Duman, Şeyma Koç, Serkan Koylan, Burcu Çam, Baran Tunç, and all the others I could not name right now. They were all supportive and friendly, and I will always remember our nice memories together. I would also like to thank Şerif Kaya for his understanding and happy mood which affected me very positively and I was glad to work with Fatih Pişkin. Furthermore, Lütfi Ağartan, Berk Doğu, Simge Tülbez, Mehmet Hazar Şeren, Sena Okay, Zeynep Öztürk, Ekin Solak, Yadigar Seymen, Gözde Öztürk, Burçin Kaygusuz, Doğancan Sarı, Sıla Ece Atabay, Ezgi Onur Şahin,

Gözde Alkan, Barış Alkan, Mete Batuhan Durukan, Doğa Doğanay and many other that I could not fit here but my heart and mind, were very friendly and supportive. I have countless memories with all of them and they will be remembered sincerely.

My friends whom I have known for the longest, Uğur Gürel, Fatih Öztürk and Kıvanç Güzey have been always there for me. Their support and belief in me have never ended. We have shared so many things together that it would be meaningless to state their role in my life. They affected the person I am today. Many years we spent together, I have learned many things from them for which I am very grateful. I am also very grateful for their love and support of my grandparents, especially my grandmother who basically raised me, my aunts, my cousins, and all my close relatives.

For all my life, my parents and my sister have always been supportive, helpful, and lovely to me. I would be unable to thank, appreciate and love them enough. They have been with and beside me, through any success, failure, stress, happiness that I have experienced. They have always trusted me and been there for me no matter what and how I do. I would not able to finish this thesis without them.

TABLE OF CONTENTS

LIST OF TABLES

TABLES

LIST OF FIGURES

FIGURES

NOMENCLATURE

Mn-Al: Manganese-Aluminum

DSC: Differential Scanning Calorimetry

VSM: Vibrating Sample Magnetometer

EDS: Energy Dispersive X-ray Spectroscopy

XRD: X-ray Diffraction

HEXRD: High Energy X-ray Diffraction

RE: Rare-earth Elements

SEM: Scanning Electron Microscopy

TEM: Transmission Electron Microscopy

CHAPTER 1

INTRODUCTION

Permanent magnets are hard magnets with high permanent magnetic properties. It is difficult to demagnetize them, therefore they are used in applications where high permanent magnetism is required. Some of the application areas can be listed as electric motors, loudspeakers, and separators. They are particularly used when the application requires a transformation of energy from one kind to another, hence they can be seen in various parts of many devices and motors.

Most of the conventional permanents magnets consist of rare-earth (RE) elements, especially Neodymium (Nd), and Samarium (Sm). In recent years, there have been several difficulties in commercially obtaining and using the RE elements. Most of the world reserves are located in a single country and due to restricted export quotas and limitations, they are not readily available and as cheap as they used to be. The difficulties in exporting these elements also affect their prices. The price of RE elements fluctuates quite frequently. Despite their magnificent magnetic properties, there occurs a requirement for alternative permanent magnets which does not contain any RE elements, or contains less amount of these elements. Therefore, developing an RE-free permanent magnet or improving an existing one has become a hot research topic recently. There are a few existing permanent magnets, i.e. Alnico and ferrites, which are available to be used in the market. However, there seems to be a huge gap between the magnetic properties of conventional RE-free permanent magnets and RE permanent magnets. Although it seems very difficult to reach the magnetic properties of permanent magnets containing RE elements, it may be possible to produce a permanent magnet with properties higher than the conventional RE-free permanent

magnets. Manganese-Aluminum (Mn-Al) alloy is a very promising candidate, which has a potential to possess higher magnetic properties than conventional RE-free permanent magnets.

This alloy has a metastable ferromagnetic phase, which occurs due to solid-state phase transformations. There are some studies in order to stabilize this τ phase. It is claimed to be originated from high-temperature ε phase. However, neither ε phase nor stable phases (β and γ_2) around the τ phase formation composition range show a ferromagnetic behavior. Thus, the composition and phase transformations are critical for this potentially permanent magnet alloy.

1.1 Thesis Organization

The main focus of this thesis study was to analyze the solid state phase transformations and the effect of composition on these transformations which leads to the formation of ferromagnetic τ phase in Mn-Al system.

In this current chapter, a brief summary of the topic has been introduced. The motivation and main points of the study were asserted.

In the second chapter, a general literature review was given. It starts with the origins of magnetism and its types, then continues with the introduction of related magnetic properties to this study. Afterward, permanent magnets, both RE permanent magnets, and RE-free permanent magnets were briefly explained. In the last part of this chapter, Mn-Al alloy, its crystal structure and microstructural aspects were shown and the phase transformations of the system were explained. The corresponding literature review was given.

In the third chapter, experimental parameters were expressed. The alloy production method, instruments used for thermal, structural, magnetic, and microstructural characterization were explained.

Results were given and discussed in the fourth chapter. The results were mainly divided into two parts. The first part of the results was about the general investigation of Mn-Al alloys. Their production and characterization were examined. Then, in-situ heating high energy X-ray diffraction (HEXRD) was introduced. Moreover, some kinetic analyses were conducted. In the second part of this chapter, in-situ heating HEXRD experiments and the relationship between composition and phase transformations were asserted in details.

In the last chapter, a general conclusion of this study was drawn and future recommendations were given.

CHAPTER 2

LITERATURE REVIEW

2.1 Magnetism

The word magnetism stems from the district Magnesia, where loadstones were found. Today we define it using the term, magnetic moments. Electron's orbital motion and its own spin around itself are the main causes of these magnetic moments. Due to the cancellation events of these moments, several types of magnetism can be observed for different materials [1-3]. The details in magnetism are given in the following sections.

2.1.1 Types of Magnetism

Magnetism may be divided into three main classes which are paramagnetism, diamagnetism, and ferromagnetism. Ferrimagnetism and antiferromagnetism are considered as subgroups of ferromagnetism.

Diamagnetism is a type of magnetism which is only observed when a magnetic field is applied. This type of magnetism occurs due to the small magnitude of magnetic moments under an external magnetic field. Alignment of the dipoles is opposite to the field direction.

In paramagnetic materials, dipoles are randomly oriented and there is not a net magnetization. These two types of materials are not regarded as magnetic because they do not possess any magnetism without an external magnetic field. Aluminum, Chromium, and Titanium are a few examples of paramagnetic materials.

In comparison with these types of magnetism, ferromagnetism shows much larger magnetization values with a permanent magnet behavior. Once the material is magnetized, even in the absence of a magnetic field, it remains magnetic. Figure 2.1 shows the dipoles of a ferromagnetic material without any external magnetic field and they are aligned parallel to each other [2, 3]. This type of magnetism is the main focus of the thesis.

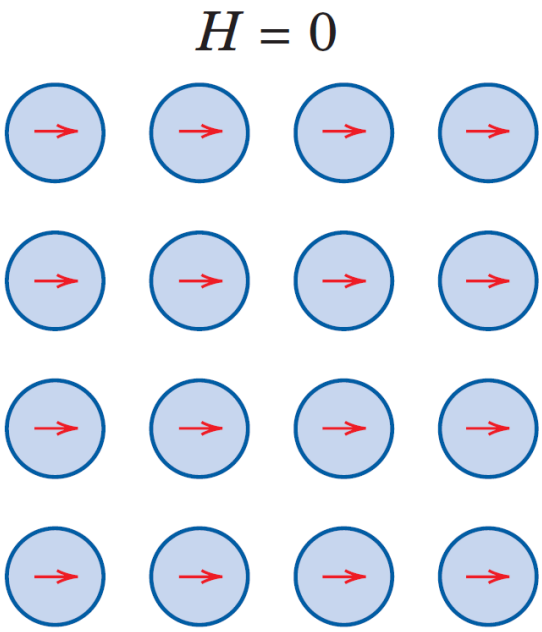

Figure 2.1 Atomic dipole orientation of a ferromagnetic material when there is no magnetic field [3].

Antiferromagnetism is somewhat similar to ferromagnetism, but it is seen due to the coupling of ions and adjacent atoms. Spin moments of neighboring atoms or ions are aligned oppositely in this case. MnO is an example of antiferromagnetic material.

Ferrimagnetism is seen on ceramics and it is similar to ferromagnetism. The difference arises from what causes the net magnetic moments. These materials may have MFe_2O_4 type formula where M is a metallic element [2, 3].

2.1.2 Domains and Hysteresis

Below their Curie temperature, ferromagnetic materials are combined by some district regions where all of the magnetic dipole moments are oriented in the same direction. Each of these district regions is called a domain. The lines where orientation changes are domain boundaries and each neighboring domain has a different direction of magnetic dipole moments. Before a ferromagnetic material is magnetized, magnetization direction differs from domain to domain which causes a sum of zero magnetization. Figure 2.2 shows how the domains get oriented when a ferromagnetic material is magnetized. During magnetization, domain boundaries move which causes differences in the sizes and shapes of domains. As the field increases, domain orientation changes accordingly and align itself along the direction applied magnetic field. At this point, only a single domain exists [3].

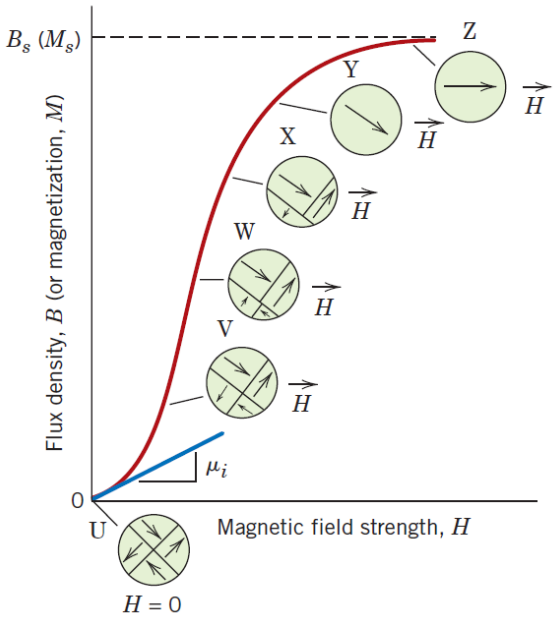

Figure 2.2 Changes in the orientation of domains during application of a magnetic field to a ferromagnetic or ferromagnetic material [3].

2.1.3 Magnetic Properties

When magnetic materials are considered, there are several important magnetic properties that should be considered. Extrinsic properties such as maximum energy product and coercivity are in relation with the real structure of a material such as size and texture of grains, whereas intrinsic properties are more dependent on the crystal structure and chemical composition which derive from the atomic origin of the material. For instance, properties such as Curie temperature and saturation magnetization are mostly affected by the transition-metal sublattice [4, 5].

In order to better understand these properties, hysteresis loop should be reviewed carefully. Figure 2.3 shows a representative B-H curve (hysteresis loop) for a ferromagnetic material. An applied magnetic field increases the magnetic flux density. As the magnetic field increases, the flux density also increases up to the point where it gets saturated. The magnetic flux density at saturation point is called saturation magnetic flux density, B_s. When the external magnetic field is removed, the curve follows the arrows as shown in Figure 2.3. The point where applied magnetic field becomes zero, there may still be some magnetic flux density removed in the material. This is called the remanent flux density, or remanence and it is shown with B_r. This shows that a material can hold magnetism without any external magnetic field. In order to demagnetize the material or in other words, to bring the value of magnetic flux density to zero, a negative magnetic field should be applied. The value of the magnetic field that should be applied to demagnetize the material is called coercivity, $-H_c$. Also from Figure 2.3, it can be seen that this magnetic field application and removal follows a hysteresis behavior. That is why it is called as hysteresis curve (B-H curve). Within this hysteresis curve, another property that can be obtained is called the maximum energy product, BH_{max}. This value can be calculated from the largest area in the second quadrant of the hysteresis curve which is a combination of both B and H. Magnetic properties are also dependent on temperature. At 0 K, the saturation magnetization value reaches to its maximum.

As temperature increases, this value starts to decrease and suddenly becomes zero at a specific temperature called as the Curie temperature [3].

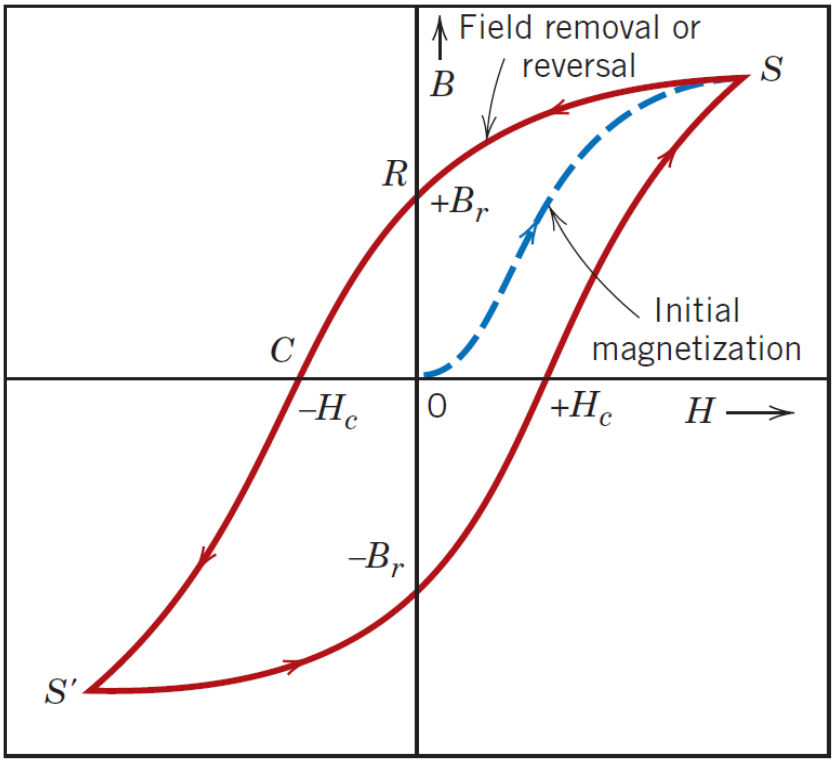

Figure 2.3 Magnetic flux density vs. magnetic field strength for a material showing a ferromagnetic behavior [3].

One other parameter that may be taken into account related to magnetic properties is magnetic anisotropy. The absolute free energy is obtained with the absence of an external magnetic field when the mean magnetic moment of a ferromagnetic material has the same direction with the crystallographic direction. That direction is easy magnetization direction and it is called as ‘easy axis’. The total free energy is dependent on magnetization direction which is affected by different crystallographic directions. This situation can be defined as magnetocrystalline free energy or magnetic anisotropy. It can also be expressed as the magnetocrystalline anisotropy. This anisotropy is therefore related to the crystal structure of the material. For permanent

magnet applications, since easy axis is a significant phenomenon, mainly tetragonal or hexagonal crystal structures are preferred [5].

Since this thesis is rather focused on solid-state phase transformations, coercivity and remanence values are frequently used in the following chapters.

2.1.4 Types of Magnets

In general, magnets can be classified into two main groups. First one is soft magnets and the second one is hard magnets. These two may be differentiated by their area of applications within the loop which can be seen in Figure 2.4. This study focuses on hard magnets which will be discussed in this chapter as permanent magnets.

2.2 Permanent Magnets

Permanent magnets are hard magnets, and they are ferromagnetic or ferrimagnetic materials which are not easy to demagnetize. They have relatively higher magnetic flux which makes them useful in a wide range of applications. They have a significant role in various machines and motor applications and they are used in areas where energy conversion is critical.

Permanent magnets can be used in several commonly used devices such as electric motors, loudspeakers, generators, alternators and other devices where the energy is transformed one form to another [6-9]. Permanent magnets are also used in magnetic forces for the application of a mechanical work, torque drives, separators, bearing and coupling devices. Synchrotron insertion devices, cathode-ray tubes, magnetrons also contain a permanent magnet to control electric charge, electron, ion beams or plasmas. They are also found in magnetic recording media for information storage and in sensors for detection [7].

The well-known permanent magnets can be classified according to the elements used in their synthesis. Two major types of the permanent magnets are the rare-earth-based

magnets (RE PMs) and rare-earth-free permanent magnets (RE-free PMs) which do not have any rare-earth elements in them.

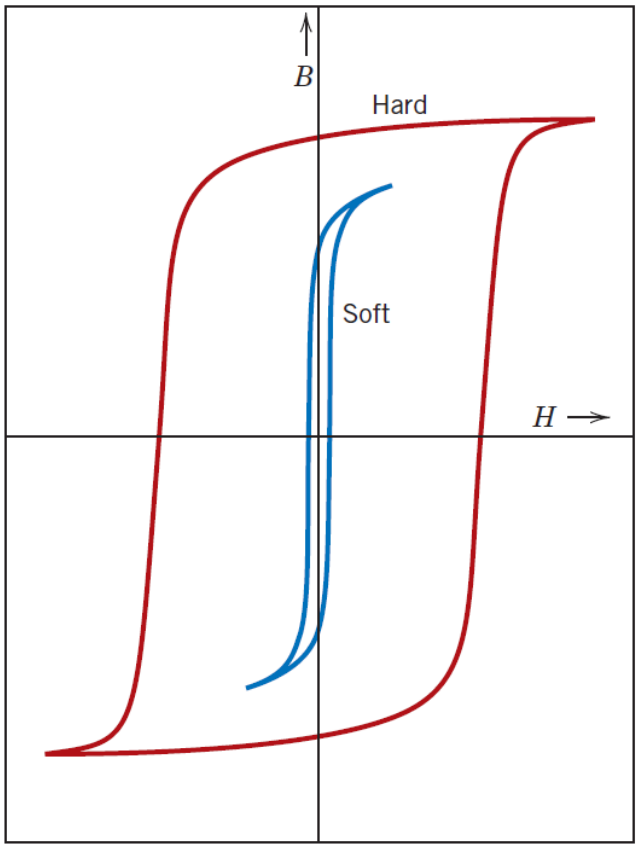

Figure 2.4 Representations of hard and soft magnets by their comparative hysteresis loops shown with different colors and name indications [3].

2.2.1 Rare-earth Permanent Magnets

As their name indicates, RE permanent magnets contain rare-earth elements which are lanthanide series elements including scandium and yttrium [10, 11]. Neodymium and Samarium are the most common ones used in these magnets. These elements provide exceptionally high magnetic properties which make these magnets used frequently in several applications.

Samarium-Cobalt (SmCo) was invented in the 1960s and it was a strong permanent magnet compared to Alnicos and ferrites. The most common magnets including Sm and Co are the $SmCo_5$ and the Sm_2Co_{17}. However, this was an expensive magnet and Samarium was not commonly available [12]. $RE_2TM_{14}B$ magnets were discovered in the 1980s. Rare-earth elements combined with a transition metal and boron are cheaper as compared to SmCo magnets. The most common type these magnets is $Nd_2Fe_{14}B$. These RE based magnets are commonly used with compositional changes and different manufacturing methods in different application areas some of which are mentioned previously. They became very popular in magnet industry [11].

2.2.2 Rare-earth free Permanent Magnets

The most well-known examples for RE-free permanent magnets are Alnico magnets and hard ferrites. These magnets do not have a magnetic matrix but they have fine ferromagnetic particles. The permanent magnets became widespread with the introduction of Alnico cast alloys and ferrite sintered alloys. Alnico alloys become magnetic with solid state precipitation of these particles. They gain their magnetic behavior due to a spinodal decomposition where a high-temperature phase composes into a FeCo-rich ferromagnetic phase and a NiAl-rich phase which is not magnetic [13]. Ferrites, on the other hand, require larger particle sizes and it is obtained by comminuting the bulk material. The most common ones are barium ferrites and strontium ferrites. In Alnicos, particles are elongated, therefore a shape anisotropy occurs and this is the reason why they are ferromagnetic. Unlike Alnico, for instance in barium ferrites, the ferromagnetic behavior is obtained from magnetic anisotropy since coupling of magnetization to crystal structure is observed. A high remanence and a low coercivity are common characteristics for Alnicos which make them susceptible to demagnetization. Moreover, they have a high Curie temperature around 850 °C. Because of the cobalt, they are rather expensive magnets, as similar to SmCo. In the case of ferrites, they have relatively low magnetic properties but higher coercivity compared to Alnico. They have a Curie temperature of 450 °C [14–16].

Even these are commonly used materials for permanent magnet applications, they have moderate maximum energy product values which mean that they have lower magnetic properties as compared to their RE-containing counterparts [17]. Figure 2.5 provides a comparison of RE permanent magnets and RE-free permanent magnets schematically. This situation makes RE permanent magnets more useful than the others. However, there are some strategical issues related to rare-earth elements. These elements are much more expensive and there are strict limitations to obtain REs commercially. Thus, a permanent magnet with RE-free constituents is strategically important to be produced. Mn-based permanent magnet alloys may be an option for producing RE-free permanent magnets with reasonable magnetic properties [11, 18].

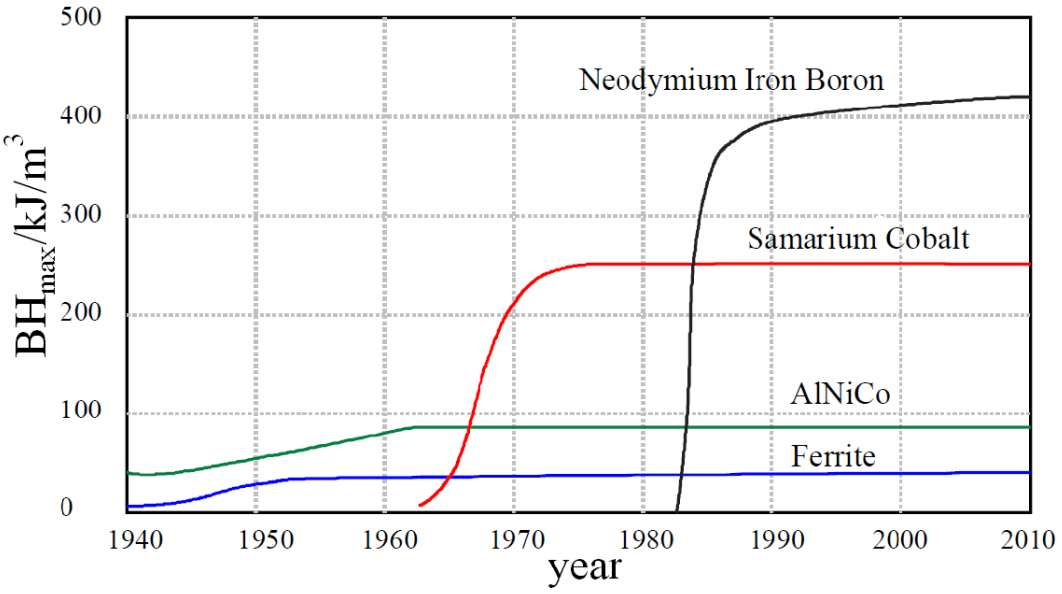

Figure 2.5 The maximum energy products of permanent magnets over the years [19].

2.2.3 Mn-Based Permanent Magnets

There are four different sites in the large manganese unit cell where Mn atoms have magnetic moments. Thus, many researchers were inspired by the large magnetic moment provided by manganese to build up a better permanent magnet. The problem

is to obtain this large magnetization values in a ferromagnetic manner with a densely packed structure. The nature of direct exchanging in the half filled “d” band is antiferromagnetic. Moreover, when the manganese orbitals hybridize, neighbors which are nearest have a tendency to get broader which reduces the magnetic moment significantly. In order to have a sufficient amount of magnetic moment, Mn atoms should be well separated. When manganese atoms are bonded with a distance larger than 290 nm, coupling becomes ferromagnetic which provides larger moments. Also, manganese is a rather cheap element which may be a huge advantage when costs and accessibility of RE elements are considered [4]. Thus, Mn-based permanent magnets can be potentially developed. The distance between Mn atoms should be well adjusted to obtain the maximum magnetic moment per unit volume and the minimum number of sites of antiferromagnetic Mn. In tetragonal L_10 and $D0_{22}$ crystal structures, this might be reached effectively [20].

There are several Mn-based permanent magnets [21, 22]. One of them is MnBi compound. This binary compound has two crystal phases which are obtained at different temperatures and called accordingly as high temperature (HTP) and low temperature (LTP) phase. The transformation between them occurs at 633 K. The LTP phase is ferromagnetic with a high uniaxial magnetocrystalline anisotropy and a high coercivity, however, HTP is paramagnetic [21, 22].

One problem that should be kept in sight related to MnBi is the cost of bismuth, which makes it challenging during mass production. Same is applicable for Ge or Ga, for instance for Mn_2Ga [23]. The structure of $Mn_{3-x}Ga$ is $D0_{22}$ and it is a continuous solid solution between Mn_2Ga and Mn_3Ga [24]. These materials have rather low magnetic moments but they may have significant coercivity values. Mn_3Ge has also similar structure and magnetic properties with Mn_3Ga [20].

The last one which will be discussed in this thesis is Mn-Al alloys. Since this thesis focused on this alloy system, it will be explained under a new title.

2.3 Phase Transformations

A brief introduction to phase transformations is given since the phase transformations in the Mn-Al system is very significant. Therefore, some basic information may provide a better understanding of the system.

When a group of atoms or molecules under equilibrium condition, which is constrained by some external parameters, are in a homogenous and have explicit physical regions, that region can be defined as a phase [25]. Each of these regions may be distinguishable due to different parameters which define density, composition, and other intrinsic properties. In order to differentiate two phases, their structure, composition or state of aggregation can be examined. With the change in external constraints, the phase may also change according to the parameters. These group of atoms always try to reach equilibrium conditions with varying constraints. The atomic structure rearranges for any phase transformation. If the solid state is investigated, it can be said that the driving forces make the reactions distinguishable. For instance, when a deformed metal recrystallizes or is exposed to subsequent grain growth, it is rather a rearrangement of atoms than a reaction. Atoms change their position due to a surface or strain energy, or an external stress. It may not be due to free energy difference only. But in all of these changes, the mechanisms of atoms are similar and related. By means of these, a transformation may be defined as the rearrangements of the structure of the atoms extensively [25].

All transformations occur due to a free energy difference which is their driving force. There occur soma fluctuations in the system from its initial state, which affects the mode of transformation. It is important that whether these fluctuations cause an increase or a decrease in the free energy. There is resistance to these fluctuations for metastable phases such that for any transformation to occur, a higher free energy path should be passed. On the other hand, a very small fluctuation which lowers the free energy makes the initial state unstable, thus the path of these fluctuations does not confront any energy barrier for transformation. The unstable phases exist temporarily,

however, if there is a limitation of atomic movement or diffusion, such a phase can be present. It is still considered as unstable because decomposition still occurs depending on the diffusion rate [25].

There are mainly two sorts of transformation based on the type of nucleation; homogeneous and heterogeneous. Most of the transformations are heterogeneous, which means the transformation does not occur throughout the system but it occurs at different parts of the system at different types. Thus, the transformation starts at different parts of the initial phase and these are the parts where nucleation occurs. For the homogeneous transformations, on the other hand, simultaneous transformation occurs at every part of the initial phase. This may be possible for some transformations such as order-disorder, in which a homogeneous or near homogeneous transformation may occur. Heterogeneous transformations can be classified in two groups according to how the temperature and time affect the transformation ratio and the rate. These are nucleation and growth type transformations and martensitic transformations. There may be some transformations with characteristics of both groups [25]. These nucleation and growth processes are thermally activated and these are diffusional transformations [26]. In nucleation and growth processes, there is generally a boundary between two phases, and the new phase grows from the previous one by transfer of atoms across the boundary. The new phase forms as the atoms migrate with a certain rate. This type of transformations is also possible for metastable phases [25].

There is another type of diffusional transformation which is called massive transformation. The phase transformations occur in a very rapid sense for some solid solutions. If the new phase forms by nucleation and growth, it is defined as massive transformation, because even it is rapid, it does not show any martensitic transformation characteristics. In these transformations, the composition does not change and the mechanism of transformation is such that at the interphase boundaries, atoms migrate in a manner of short-range diffusion. The final phase formed after massive transformation might in equilibrium or there may be supersaturation. The

kinetics of massive and martensitic transformations are very similar. Also, there are some alloys which may transform by both of them [25, 27].

Before explaining martensitic transformations, a general definition of diffusionless transformations should be given. In the diffusionless type of solid-state transformations, there is no requirement of atoms to diffuse in long-range. Rather, small atomic movements are enough for the transformation [28].

In the martensitic transformations shear mechanism is observed, and they are not thermally activated. The crystal structure may be different from the initial phase but they are compositionally invariant or degree of ordering does not change [25, 27]. Martensitic transformations only occur in solid phases. They are considered as diffusionless (they is no requirement of long-range diffusion) and the composition does not differ before and after the transformation. The transformation begins spontaneously which causes the initial phase to be mechanically unstable. At a certain temperature, a very rapid transformation occurs. Initial phase turns into the final phase until it is all transformed which is the primary characteristic for this type of transformation. Martensitic transformations have high reversibility. Deformation of the system is more significant for martensitic transformations than nucleation and growth transformations [25].

2.3.1 Kinetic Analyses (Kissinger and Ozawa Approaches)

Activation energies of phase transformations can be found from isochronal differential scanning calorimetry (DSC) scans. Two prevalent approaches for this are Kissinger [29] and Ozawa [30] approaches.

Kissinger method is an approach which is used for determination of activation energies of first order phase transformations. Some phase transformations require a certain activation energy to occur. When this situation happens, a thermal energy is required to overcome the energy barrier which means the transformation requires a thermal activation. This also means that heating rate has a significant effect on the reaction. As

the heating rate changes, the temperature at which the transformation occurs changes. Therefore, at a certain heating rate, the peak temperature on a DSC signal for a phase transformation should be the same and as the heating rate changes, the peak temperature changes. It is asserted that the maximum rate of an exothermic reaction is assumed to be obtained at its peak temperature. Therefore, the activation energy can be calculated at different heating rates which affect the transformation temperatures [29]. The following equation can be used to calculate an exothermic reaction's activation energy:

$$\ln\left(\phi/T_p^2\right) = const.\left(-\frac{E_c}{RT_p}\right) \qquad \text{Equation 2.1}$$

where ϕ is the heating rate, T_p is the peak temperature of the transformation, and E_c is the activation energy of the reaction. This formula can be used to determine the activation energy of the phase transformation. When $\ln(\phi/T_p^2)$ versus $1/T_p$ is plotted, the slope of the linear fit of this plot gives the activation energy of an exothermic phase transformation.

The activation energy of a reaction can also be calculated using Ozawa's approach. This approach is pretty similar to the Kissinger's except one assumption related to the kinetics of the reaction. Ozawa indicates that changing the heating rate would not affect the order of the reaction [30]. As the order stays constant, a different equation is used for determination of the activation energy of an exothermic phase transformation:

$$\ln(\Phi) = const\ \left(-\frac{1.052E_c}{RT_p}\right) \qquad \text{Equation 2.2}$$

where ϕ is the heating rate, T_p is the peak temperature of the transformation, and E_c is the activation energy of the reaction. For this method, $\ln(\phi)$ versus $1/T_p$ plot is used. As a linear function is fitted to the plot, the slope of that linear fit again gives the activation energy of the exothermic phase transformation.

2.4 Literature Review on Mn-Al system

The Mn-Al system consists of many phases as it can be seen in Figure 2.6. What makes this system useful for magnetic applications is the composition range of 50-60 atomic percent manganese (approximately 67-75 weight percentage). In this range, there is a metastable, ferromagnetic τ-phase, which makes Mn-Al alloys a potential candidate for permanent magnet applications. τ-MnAl phase is ordered, it has a Curie temperature of 635 K and a magnetic moment of 1.94 μ_B. It has a high uniaxial magnetocrystalline anisotropy value of 93 x 10^4 J/m^3 which is quite unusual for RE-free permanent magnets [31, 32].

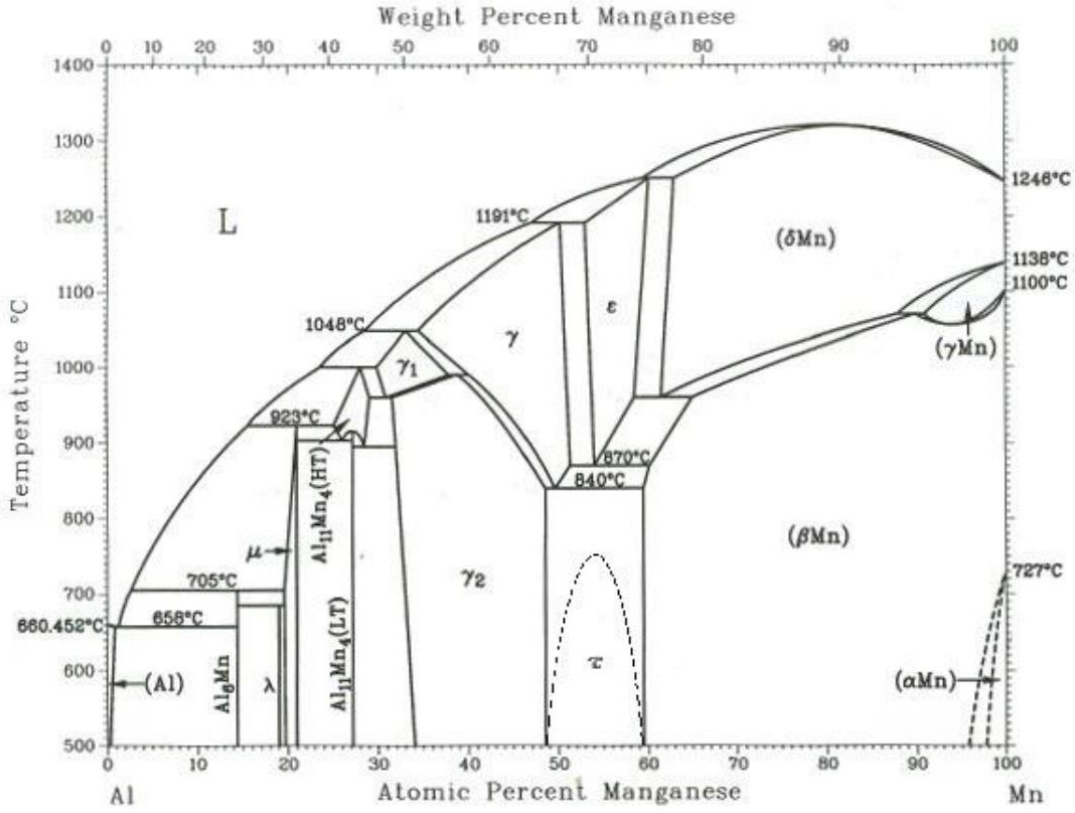

Figure 2.6 Al-Mn phase diagram [40] which is adapted from [42].

The crystal structure of τ-MnAl phase can be seen in Figure 2.7. On the top left, the face-centered unit cell is shown which has the AuCu structure type [33]. Dashed lines is a simpler designation of the structure. This is a primitive tetragonal lattice with lattice constants of; a = 2.77 Å and c = 3.54 Å. It can be considered as a distorted cubic cell (bottom of the figure) [32].

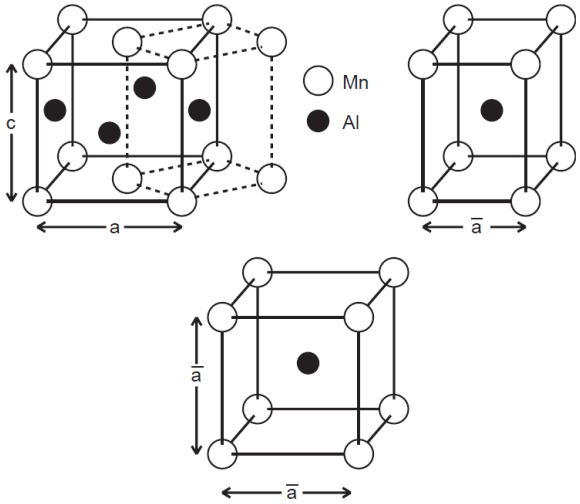

Figure 2.7 Crystal structure of τ-phase in the Mn-Al system. Dashed lines are for reduced tetragonal which is separately shown on top right. At the bottom, the idealized cubic structure is shown [32].

In the τ phase region, there are also other phases. High temperature phase is ε phase which has an hexagonal structure ($P6_3/mmc$ space group) with lattice constants of; a = 2.69 Å, and c = 4.38 Å, stable β-Mn phase which has a cubic structure ($P4_132$ space group) with lattice constant of; a = 6.315 Å, and stable γ_2 phase which has a orthorhombic structure (R3m space group) [34]. The τ-MnAl phase has L_10 structure. There have been several studies related to the L_10 structure magnetic alloys. Alloys such as Fe-Co and PtCo and some of their derivatives consisting of other elements (Rh, Pd, Ir, Pt with; Mn, Fe, Co, Ni) were previously investigated [35]. Some research has been done on the coercivity of FePd alloy [36]. However, most of these elements are not comparable with RE permanent magnets in terms of magnetic properties and

price. L_10 τ-MnAl is both has the potential of high magnetic properties [37] and it is cheaper due to elements used in the system. This tetragonal crystal structure is ferromagnetic due to manganese magnetic moments in terms of τ-MnAl phase. Manganese spins are exchange coupled to be parallel and this intermetallic phase has a high uniaxial magnetocrystalline anisotropy which related to these moments and the easy c-axis [38, 39]. In Figure 2.8, the configuration of moments and easy axis can be observed. The phase diagram in Figure 2.6 shows the estimated composition range where τ-phase forms [40]. Since it is not stable, if formation does not occur as it should have been, β-Mn and γ_2 phases form instead of τ phase. Despite thermodynamically stable phases are observed at room temperature, the metastable τ-phase may transform from high-temperature ε-phase by several routes [38]. These will be discussed in detail in the following parts.

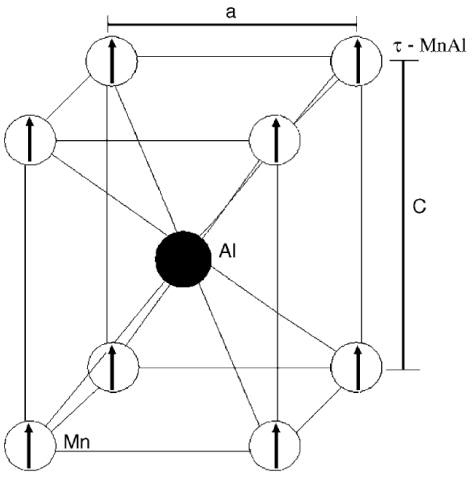

Figure 2.8 Structure of τ-MnAl phase which has L_10 configuration showing the Mn spins at the corners [41].

This alloy system has been studied by many researchers in many different ways. Production method, heat treatment parameters, characterization methods, computational methods, compositional differences have been all studied. First one is related to the production of these alloys. Several methods of production have been

tried and they have been compared. Some of these methods are casting, induction melting, arc-melting, mechanical milling, warm extrusion gas atomization, melt spinning, and rapid solidification rate processing [43-52]. They were also produced as films and bilayers [53-56] and a carbon including study used drop synthesis method [57]. Moreover, some methods such as cryogenic milling [58] and spark plasma sintering [59, 60] were also studied. Depending on the production method used, these alloys can show different properties due to microstructure, morphology, and size of the grains of the specimens.

Various computational methods were used to obtain information about the system such as linearized augmented plane wave method [37, 61]. The ferromagnetic instability of Mn-Al system was studied by using an ab-initio density functional based Korringa-Kohn-Rostoker (KKR) method [62]. Some calculations were made with a frozen-core full potential projected augmented wave (PAW) method on Fe-doped Mn-Al alloys [63]. These methods provide significant information for understanding the system, its potential, limits, and properties.

The heat treatment procedures of Mn-Al alloys were studied in detail in order to obtain ferromagnetic τ phase from high-temperature ε phase. The most common explanation for the formation of τ phase from ε phase is that the alloy is solutionized at ε phase region and then quenched in order to obtain single ε phase at room temperature which is the commonly used method [41, 64, 65]. Then with a second heat treatment at 300 °C (573 K) – 700 °C (973 K) is applied for different periods of time [41, 53]. This second heat treatment causes the transformation from ε phase to τ phase.

However, it may also result in the formation of stable phases rather than achieving single ferromagnetic τ phase. This τ phase is a metastable phase [38], and there are some problems related to the volume fraction of τ phase obtained [62]. There are these stable phases (β and γ_2) on the phase diagram which may form during the heat treatment procedure. Thus, studies related to Mn-Al system, its phase transformations,

third element additions should be regarded in more detail which will be done in the next parts of this chapter.

In the respect of investigating this ferromagnetic phase, there are several studies in the literature. It can be said that parameters such as production route, heat treatment parameters, defects, crystallite size have an effect on the magnetic properties of Mn-Al alloys. The defects in the alloy and the size of ε phase crystallites have an effect on the magnetic properties and τ phase formation of the system. The production route seems to have an effect on the amount of τ phase. Since mechanical alloying causes smaller grain sizes in the microstructure, methods such as arc melting on the opposite, result in the largest grain size with the highest fraction of τ phase. The best magnetic properties were achieved with a sample produced by a combined method of arc melting and ball milling. Curie temperature was found as 365 °C (638 K), the coercivity value was measured as 1.8 kOe and a remanence value about 16 emu/g was obtained. The defects of the system have also an effect of pinning the ferromagnetic domains which can be related to the magnetic property improvement. These may also act as the sites where the τ phase nucleates [45]. Bittner et al. (2015) observed the defects of the system by EBSD [66] (Figure 2.9). Foreback et al. (2008) asserted that they achieved the optimum magnetic properties with a composition of 54 at% manganese, after it is annealed at 400 °C (673 K) and resulted in a 300 μm average grain size [67]. It is also asserted by Zeng and Baker (2006) that, the amount of τ phase and the size of grains have a strong effect on the magnetic properties of the alloy. They produced a nanocrystalline microstructure by mechanical production methods i.e. alloying and milling. They claimed much higher magnetic properties. 4.8 kOe coercivity and 87 emu/g remanence values were reported for the alloy with the same composition and by using the same heat treatment temperature for 10 minutes [68]. The temperature at which the transformation of ε phase to τ phase occurs showed a decrease of 100 K because of fine grains of ε phase in an alloy with a composition of 55 at% Mn [69].

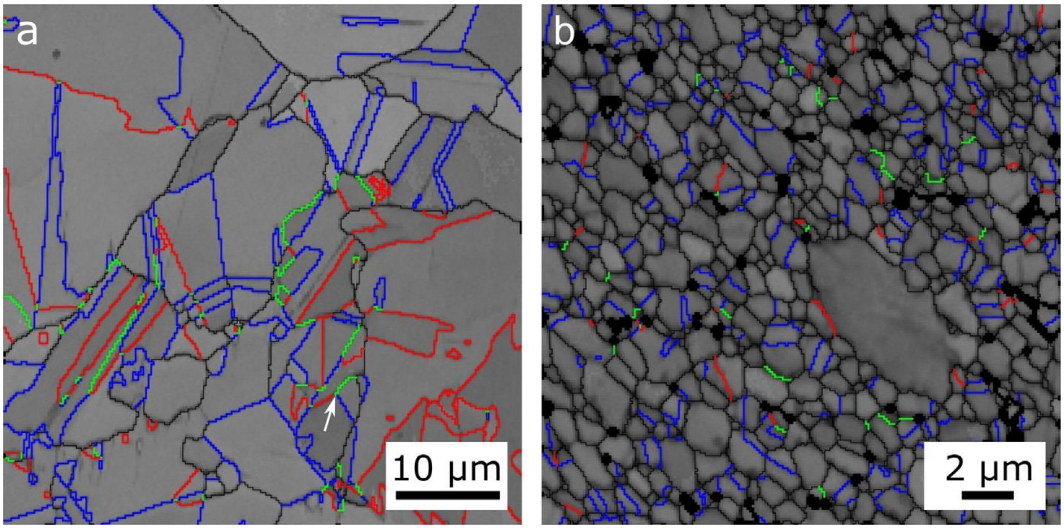

Figure 2.9 Representation of {111} interfaces distributed spatially for (a) as-transformed and (b) hot extruded sample. All colors represent a defect; order twins (red), true twins (blue), pseudo twins (green), and grain boundaries (black) [66].

2.4.1 Phase Transformations in Mn-Al system

The phase transformations in the system are explained briefly with several examples from the literature. It is important to understand how the τ phase occurs in order to improve the magnetic properties. Three main theories can be seen in the existing studies related to the mechanism of the transformation of ε phase to τ phase.

In the first theory, it was claimed that the phase transformation occurs in two steps. The ε parent phase (A3) first orders into an ε' (B19) phase. Then, the ferromagnetic τ phase (L_10) forms due to a displacive or martensitic shear of this ε' phase [39, 70- 74]. This theory can also be seen in Figure 2.10. It was asserted that the parent ε phase consists of some ε' phase nuclei when it first forms. Thus, during the heat treatment, the ordering step occurs and ε+ε' phase mixture matrix reveals stacking faults with high density which causes the martensitic shear process resulting in the formation of τ phase from the ε' phase. In a later investigation, it was seen that together with martensitic shear, a reordering transformation which requires thermal activation occurs during the second step of the transformation [74].

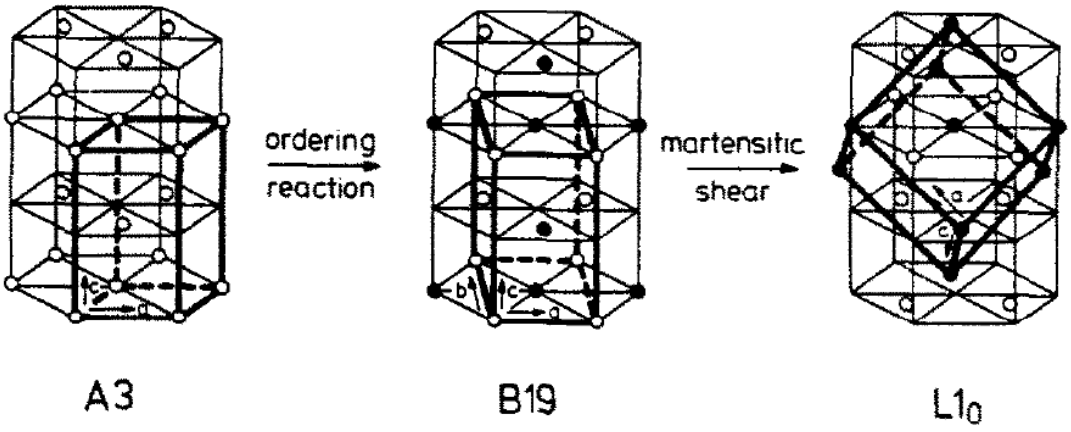

Figure 2.10 The illustration of the theory which shows the relationships between the lattices of the phases A3 (hexagonal), B19 (orthorhombic) and $L_1 0$, (tetragonal). Close packed planes are oriented parallel in the drawings [39].

A massive transformation during the heating operation was asserted as the second theory. This massive transformation was observed to be invariant of composition and it is a diffusional transformation [38, 75–77]. Between a temperature range of 450 °C (723 K) - 700 °C (973 K), heterogeneous nucleation of τ phase occurs at the grain boundaries and the growing of the phase happens behind the advancing incoherent interfaces [75]. Electron microscopy observations showed that there was a lot of lattice defects such as dislocations and twins in the resultant microstructure of τ phase (Figure 2.11) [76]. There were several defects found in ferromagnetic τ phase during the microstructural investigation of the alloy such as arrays of overlapping octahedral stacking faults, microtwins, thermal antiphase boundaries, and dislocations. There was the migration massive growth interface, and at the interface, these defects originate with an atomic attachment on {111} and {020}-type facets [77]. The growth mechanism includes random jumps of atoms from the parent phase at the nucleation sites. This behavior was explained by the classical nucleation theory. There is also a relevance between the activation energy calculations and the interphase boundary diffusion [38].

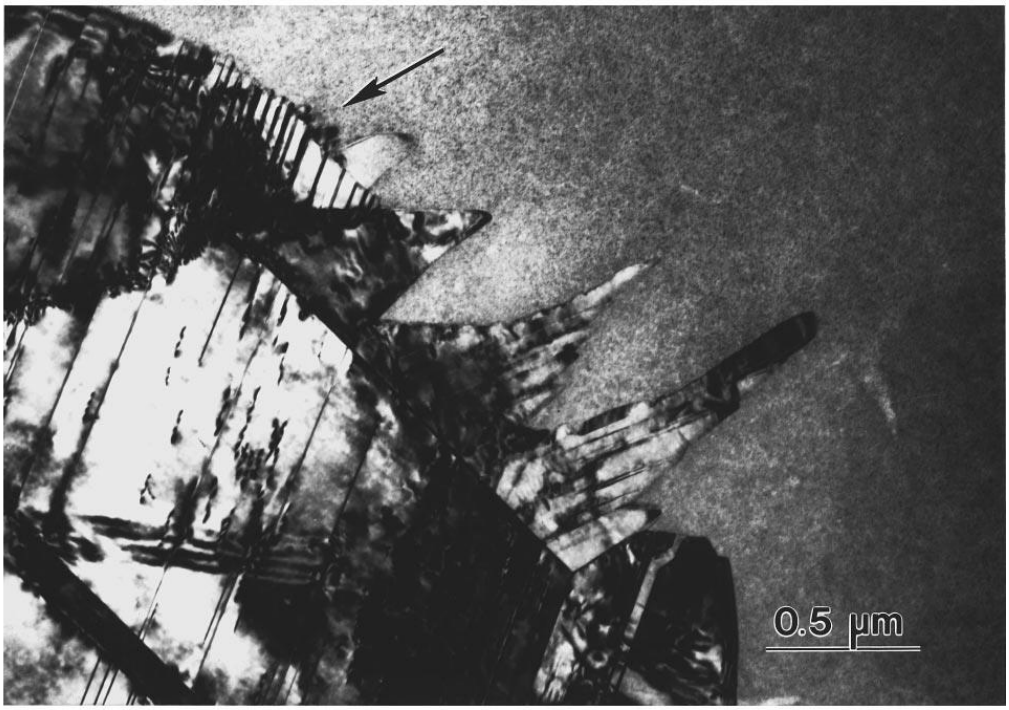

Figure 2.11 Bright-field TEM image of an ε/τ interface showing the development of the polytwin structure and the nucleation of new twin variants which is pointed out by the arrow. Specimen aged 15 min at 450 °C [76].

The third theory was claimed by Wiezorek et al. (2011). There is both structural shear and atomic diffusion in this new mechanism of the transformation and it was called as hybrid displacive-diffusional transformation. They have performed detailed transmission electron microscopy (TEM) analysis to support this mechanism and showed both displacive shear mode and the diffusional massive mode (Figure 2.12 and Figure 2.13). It was asserted that the transformation kinetics are controlled by the massive transformation mode, whereas partial dislocation glide causes the τ phase formation. It was shown by TEM images that ε' phase and ε phase coexist in the same matrix. It was said that ε' phase is present due to the initial elastically accommodated anisotropic misfit strain. Stacking faults overlap each other which were observed in the ε + ε' matrix which causes the formation of τ phase. This was also supported by

in-situ heating TEM imaging and it shows that there are lots of twins and stacking faults on the close-packed planes of ferromagnetic τ phase [78].

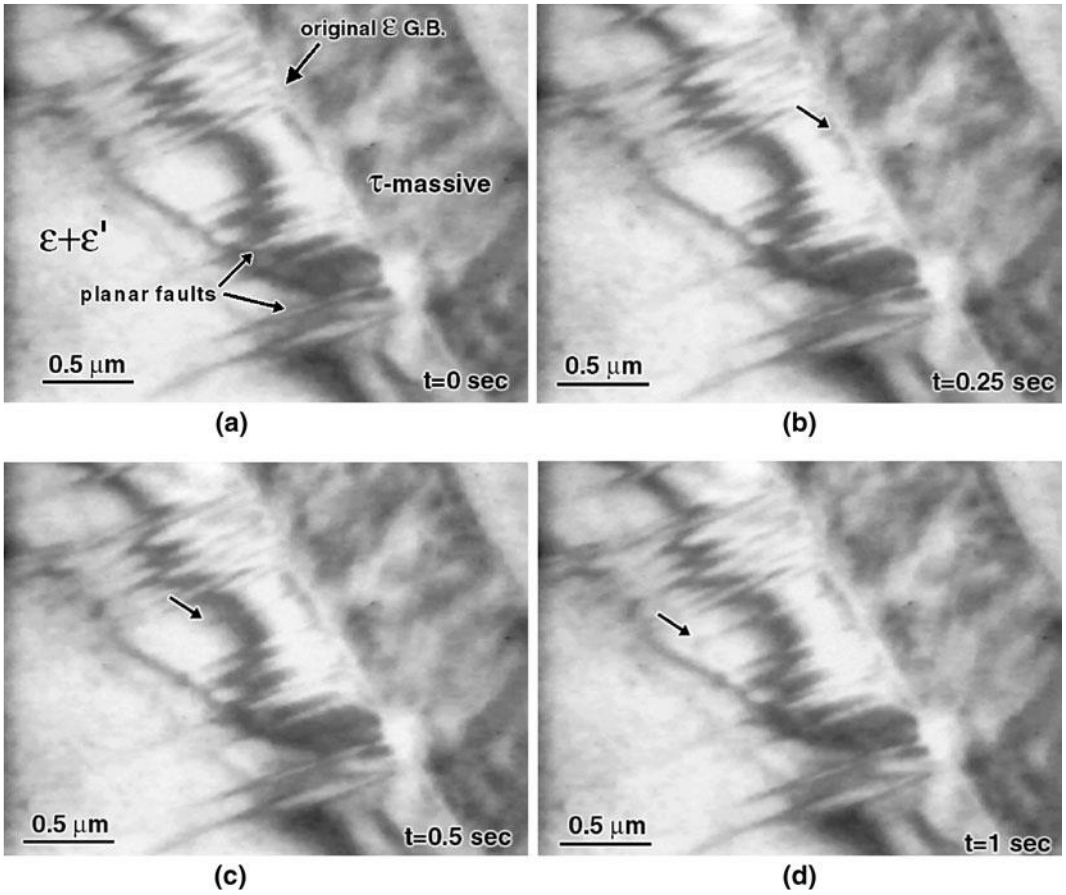

Figure 2.12 Some of the frames taken from an in-situ heating TEM experiment. This shows how the planar faults nucleate at the interface of massive τ-product [78].

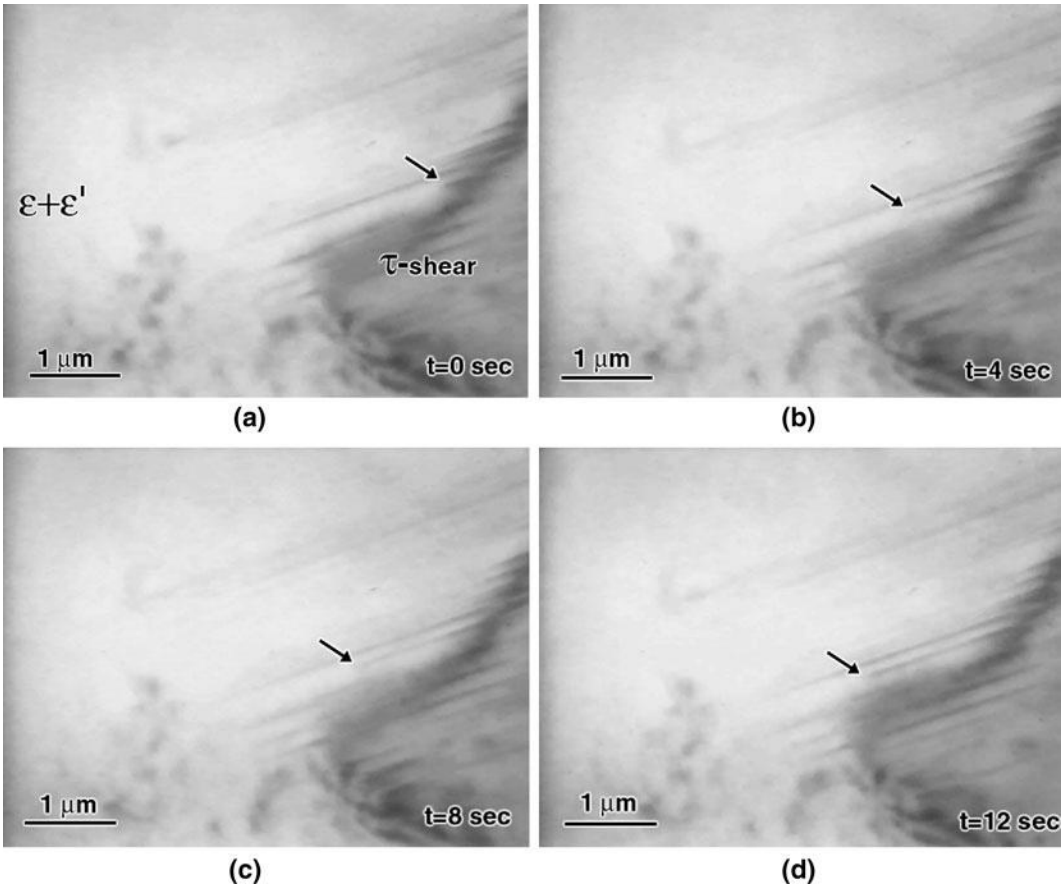

Figure 2.13 The plate-like τ phase grows into the ε + ε' phase mixture which is formed due to the shear mode [78].

2.4.2 Addition of a Third Element

There are many studies which concentrated on the development of the metastable τ phase in these alloys by the addition of impurity elements. These are generally studied in accordance with parameters like the composition and the heat treatment parameters (i.e. time and temperature). Therefore, there are also other focus points rather than the third element composition. These studies have shown that when a third element besides Mn and Al is added to the system such as C, B, Zn. Ni, Cu, and Ti, stabilization of the metastable τ-phase may be obtained generally by preventing the formation of stable phases [38, 79, 80].

Crew et al. (1995) studied three different compositions of MnAlC alloy; A(70 wt.% Mn, 30 wt.% Al), B (70.7 wt.% Mn, 28.2 wt.% Al, 1.1 wt.% C), C (72 wt.% Mn, 27 wt.% Al, 1 wt.% C) produced by mechanical alloying. Different milling times were applied for these alloys for their mechanical alloying process. The alloys A and B had a milling time of 24 hours and the alloy C had a milling time of 16 hours. This study showed the best magnetic properties for the alloy B for 10 minutes of aging at 600 °C (873 K) and the related magnetic properties M_s (saturation magnetization), M_r (remanence magnetization), H_c (coercivity) and $(BH)_{max}$ (maximum energy product) were claimed as 442 kA/m, 203 kA/m, 271 kA/m and 10.3 kJ /m^3, respectively [73].

Wysłocki et al. (1999) studied a similar composition of MnAlC alloy (73.0 wt%, 26.4 wt%, and 0.6 wt% of Mn, Al, and C, respectively) and asserted that high magnetic field measurements up to 140 kOe were reached in 4.2-283 K temperature range. They also reported that the hexagonal parent ε-phase is antiferromagnetic [81].

Yanar et al. (2001) investigated the defects of τ-phase using transmission electron microscopy (TEM) in $Mn_{54.3}Al_{44}C_{1.7}$ alloy. They reported τ-MnAl based permanent magnet alloys' magnetic behaviors are strongly sensitive to its defect structure [77]. Later, Fazakas et al. (2007) investigated the $Mn_{54}Al_{44}C_2$ ribbons using differential thermal analyzer (DTA), differential scanning calorimeter (DSC) and X-ray diffraction (XRD) techniques. The thermomagnetic measurements were studied as well. The results showed an almost constant Curie temperature of 247 °C (520 K) for this alloy [82].

Zeng et al. (2007) have studied the composition effect on phase transformation and magnetic properties in mechanically milled $Mn_{50+x-y}Al_{50-x}C_y$ (x = 0, 2, 4, 6, 8; y = 0, 1.7, 3) powders. These powders were annealed in a temperature range of 350 °C (623 K) to 600 °C (873 K) for obtaining τ-phase. This study stated that the optimum magnetic properties in carbon-free $Mn_{54}Al_{46}$ alloy was the one annealed at 400 °C (673 K) for 10 minutes and the values of H_C and M_r as 4.8 kOe and 45 emu/g,

respectively were submitted. However, the highest coercivity value was obtained as 5.2 kOe in $Mn_{51}Al_{46}C_3$ powders that were annealed at 500°C (773 K) for 30 minutes [41].

Kohmoto et al. (2011) later investigated the effect of alloying time and composition on magnetic properties in mechanically alloyed $MnAlC_x$ (60, 55, 50 at.% Mn-bal. Al and x at.% C- (55-0.5x) at.% Mn-bal. Al (x=0, 2, 4, 6) and reported better magnetic properties for 10 h milling than that for 200 h. milling [83]. Recently, Liu et al. (2012) studied $Mn_{55-x}Al_{45}C_x$ (x=0, 1, 1.7 and 2), $Mn_{53.5}Al_{45}B_{1.5}$, and $Mn_{52.3}Al_{45}C_{1.7}RE_1$ (RE =Pr or DY) alloys and they asserted the highest magnetic properties for $Mn_{55-x}Al_{45}C_x$ (x=1.7). They submitted the values of J_S = 0.83 T, J_r = 0.30 T, H_{cj} = 123 kA/m, and $(BH)_{max}$ = 12.24 kJ/m^3 for the alloy annealed at 650 °C (923 K) [80]. Ohtani et al. (1977) obtained B_r = 6100 G, H_c = 2700 Oe and $(BH)_{max}$ = 7.0 MGOe with a billet of composition 70.01 wt.% Mn, 29.48 wt.% Al and 0.51 wt.% C [70].

Similarly, Sakka et al. (1989) introduced elements such as B, Zn, Ni, Cu and Ti to the Mn-Al system produced by rapid solidification. They found that alloys with Ti were more ductile and the doped ones were brittle. They compared the magnetic properties in terms of composition, annealing time and annealing temperature [79].

2.5 Motivation

Both RE permanent magnets and RE-free permanent magnets were introduced in previous sections. It was asserted that RE permanent magnets have significantly high magnetic properties, however, their strategical importance bears the need for the development of new RE-free permanent magnets with sufficiently high magnetic properties as compared to the conventional RE-free permanent magnets. Although it would be very difficult to reach up to the outstanding magnetic properties of RE permanent magnets, it is possible to improve a RE-free permanent magnet which may fill the magnetic property gap between the conventional RE PMs, and conventional

RE-free PMs. The gap is shown by comparing the magnetic properties of these permanent magnets in Table 2.1.

Table 2.1 Magnetic properties (coercivity and remanence) of conventional RE PMs and RE-free PMs (Retrieved from [84]).

Type	Permanent Magnets	Coercivity (Oe)	Remanence (kG)
Rare-earth	Nd-Fe-B	5400 - 11000	6.9 – 12.0
	RE-Co	6700 - 9000	8.0 – 11.3
MAGNETIC PROPERTY GAP			
Rare-earth Free	Alnico	440 - 1600	5.2 – 13.2
	Ferrite	1800 - 3150	1.4 – 4.0

It can be deducted from all of the information given in previous sections that Mn-Al alloys arouse interest for development. It is possible to fill the gap shown above with improvement of these alloys by obtaining higher amounts of τ phase with prevention of stable phase formation. Although the magnetic properties are very significant for permanent magnet applications, the metastable τ phase formation should be investigated in order to reach these magnetic properties. Thus, the effect of composition, heat treatment parameters, addition of other elements, stabilization of the system, and the phase transformations in the system should be studied carefully in details. In this respect, this study focuses on the kinetics and mechanisms of the phase transformations in the Mn-Al system, which yields the formation of ferromagnetic τ phase.

CHAPTER 3

EXPERIMENTAL PROCEDURE

In this chapter, detailed information about the preparation and production of alloys are given. The heat treatment procedure and characterization methods are explained in details.

3.1 Production of Alloys

The alloys were produced using pure elements. Elements were obtained from Alpha Aesar with high purities (99.95% Mn, 99.8% Al). These elements were first weighed separately and they were put together in the chamber of a copper hearth electric arc melting furnace. For this purpose, Edmund Bühler Compact Arc Melter MAM-1 in Çankaya University (Ankara, TURKEY) was used (see Figure 3.1). All of the alloys were melted under argon atmosphere for three times in order to ensure compositional homogeneity.

First, bulk samples were used as manganese pieces and aluminum shots. However, using these forms of metals, problems occurred during melting. When the arc hit the manganese pieces, they were shredded into pieces and scattered in the furnace. It was thought that this situation was due to possible oxidation of manganese pieces and their surface. Due to this reason they were cleaned and a shiny surface was obtained by using nitric acid diluted to 5.9%. The pieces were held in nitric acid for different time periods related to the condition of the piece. It was generally changing in a range of 10-40 seconds. After taking the pieces out, each of them was washed with water and ethanol and then dried. After this process, elements were again weighed and melted in

the arc furnace. The situation related to manganese pieces was occurring less with this method, but it was still a significant issue.

Figure 3.1 A capture of alloy production in an arc melting furnace.

These issues caused significant changes in composition. Composition difference was expected up to some extent, however, it was not possible to produce an alloy in the desired range with this scattering problem. Therefore, a solution should have been found. After that, alloys were produced as following:

- Rather than aluminum shots, aluminum powder with a size range of -40+325 mesh was used.
- After manganese pieces were cleaned, they were crushed using hardened steel mortar and pestle.

- Both elements were weighed in powder form and then put together in a 15 mm die.
- The die was put under a hydraulic press with a maximum load of 30 tons (see Figure 3.2) and pressed.
- The consolidated mixture has a pill like shape with 15 mm which is a cylinder similar to the die's shape with a smaller height.
- Finally, the consolidated mixture obtained was put in the arc melting and the alloys were produced in that fashion.

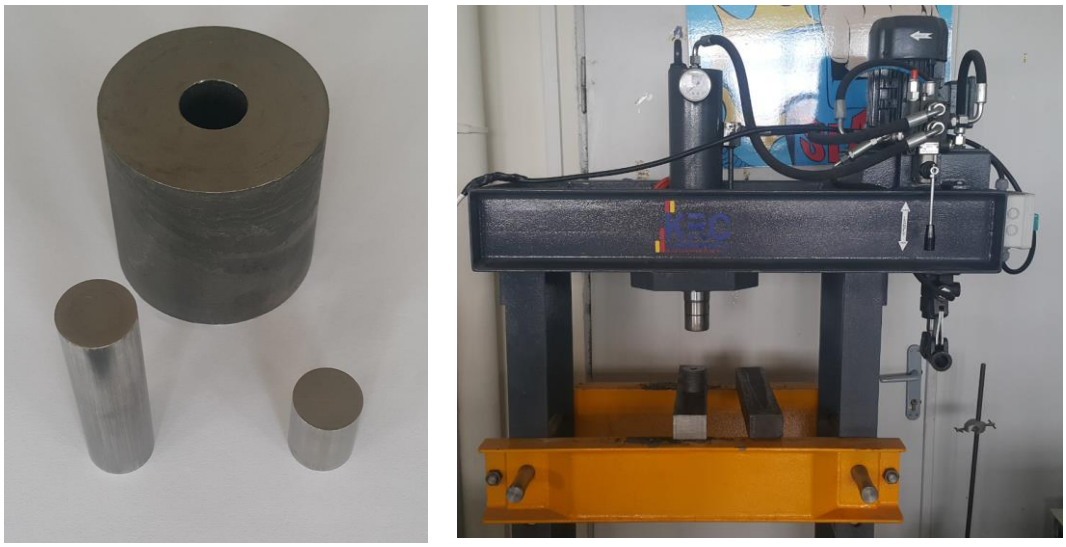

Figure 3.2 Equipment used for pressing. The 15 mm die on the left and the hydraulic press with a maximum load of 20 tons on the right.

The procedure explained above were much more useful than the previous one. The manganese losses were still observed, but the scattering issues were resolved. This provided an opportunity to study in a specific composition range.

The alloys were generally produced with a weight of 2-3 grams. Some of the samples were characterized right after the production and before the heat treatment (solutionizing) process. A larger sample in the as-melted case might have had different cooling rates which may have affected the phases present in the sample.

After the alloy production, there was a thin layer of oxide due to manganese content in the alloy. By using an 80 mesh emery paper, the outer surface of the alloys was grinded and a bright metallic surface was obtained.

3.2 Heat Treatment Procedure

Some of the as-melted alloys were directly taken to the structural and microstructural analyses. The first heat treatment procedure was applied right after the alloy production for most of the alloys.

A regular furnace was heated up to 1150 °C (1423 K) and the alloys were put in the furnace. They were held in the furnace for an hour and water-quenched subsequently in order to obtain the single ε phase. Alloys were grinded roughly for metallic surfaces. Although, this heat treatment procedure was performed under atmospheric conditions, EDS showed no sign of undesired elements. Therefore, this procedure became routine for all of the alloys after they were melted.

The second step heat treatment was applied using differential scanning calorimetry (DSC) and it is explained in details in section 3.4.

3.3 Microstructural Analyses

In order to analyze the microstructure and composition of the samples, optical microscopy and scanning electron microscopy (including EDS) were used.

3.3.1 Sample Preparation

Conventional sample preparation techniques for metallography were used for all of the samples. For compositional analysis, samples were not etched. Firstly, manual grinding was applied using 120, 200, 400, 600, 800, 1200 and 2000. Then, for polishing the specimens, COL-K (NC) polishing slurry (final polishing of nonferrous materials) was used. After polishing, specimens were etched. For this purpose, Keller's

Reagent (5 ml nitric acid, 3 ml hydrochloric acid, 2 ml hydrofluoric acid, and 190 ml distilled water) was used.

3.3.2 Optical Microscopy Analysis

Optical microscopy was occasionally used for this study. It was generally used to observe whether the samples reveal desired phases or not. After the samples were prepared for examination Huvitz Digital Microscope HDS-5800 was used to capture the optical micrographs.

3.3.3 SEM Analysis

SEM was used frequently for composition analysis. SEM micrographs were taken to observe critical microstructural features using FEI NanoSEM 430 Field Emission Scanning Electron Microscope (SEM). Sample preparation is the same as for optical microscopy analysis. Micrographs were mostly taken as secondary electron images by using Everhart-Thornley Detector (ETD).

EDAX SSD Apollo10 Detector with EDAX Genesis 6.0 Analyzing Software was used for composition analysis. The detector was attached to SEM. Energy Dispersive X-Ray Spectroscopy (EDS) was used with 6.0 spot size and data were collected for 60 live seconds. For SEM analysis, an operating voltage of 20 kV was used.

3.3.4 TEM Analysis

In order to investigate the samples under transmission electron microscope (TEM), JEOL 2100F-FEG TEM was used with an operating voltage of 200 kV. Techniques such as bright-field (BF) imaging, dark-field (DF) imaging, and selected area electron diffraction (SAED) were used. INCA X-sight Model 6498 LN2 Cooled Detector was used in order to confirm composition. TEM samples were prepared using Focused Ion Beam (FIB) at Sabancı University.

3.4 Thermal Analysis

Thermal characterization of all samples was conducted with a differential scanning calorimetry SEIKO SII X-DSC7000. Samples were put into the device in aluminum crucibles with an aluminum reference. Both powder and bulk samples were used in accordance with the purpose of the experiment. Specimens for DSC were weighed to be 10 mg, however, for some cases higher amount of specimen was used. The samples were heated under N_2 atmosphere. The N_2 gas flow was between 20-40 cc/min. Generally, samples were heated up to 500 °C (723 K) isochronally. Some isothermal studies between 300-500 °C (523 - 723 K) were also conducted. All of the samples except the kinetic analyses samples were heated up with a 10 K/min rate.

3.5 Magnetic Property Measurement

Magnetic properties were determined using vibrating sample magnetometer (VSM). These measurements were not conducted with only one VSM, but several of them were used due to technical issues. One of them can be seen in Figure 3.3, which is Cryogenic Limited PPMS (VSM device) in Central Laboratory, METU. Mostly powder samples were used with around 100 mg weight. They were immobilized with epoxy and then measured under 1 Tesla of applied magnetic field. For some other experiments applied field was different within a range of 1-5 T. Coercivity and remanence values were calculated from the experimental hysteresis loops. Each batch of samples' magnetic properties was measured with the same device, hence they were comparable with each other in that part of the study.

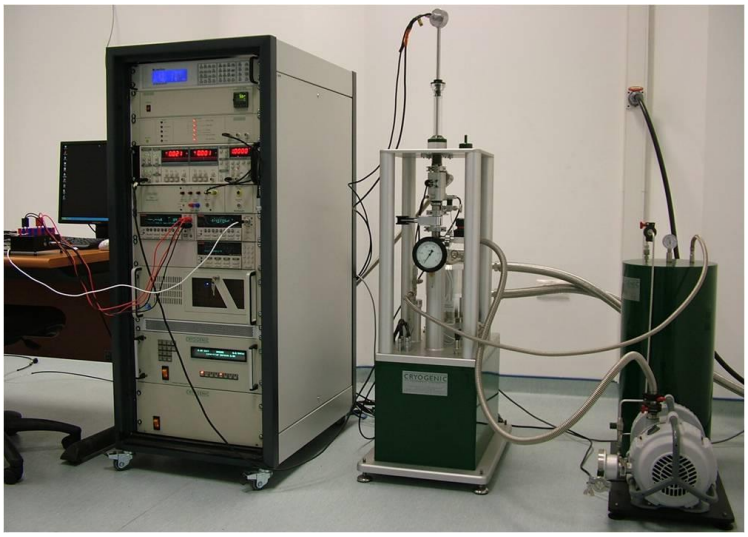

Figure 3.3 Vibrating sample magnetometer (VSM) in Central Laboratory, METU-Ankara, TURKEY (Cryogenic Limited PPMS).

3.6 Structural Analysis

X-ray diffraction (XRD) was conducted by Rigaku Ultima IV and Bruker D8 Advance diffractometers. Both of them were using Cu-Kα radiation (wavelength of 1.54056 Å). Bragg-Brentano geometry was used in all experiments. Most of the patterns were obtained between 5° - 95° with a step size of 0.02°. Scanning rate was variable but generally, 1°/min or 2°/min was used. Bulk sample data were collected with parallel beam geometry. Most of the samples were in powder form. For some samples, a heating attachment was used and some in-situ heating XRD experiments were conducted with Bruker D8 Advance diffractometer. The heating rate was 10 K/min and samples were heated up to 750 °C (1023 K). There were different steps that data were collected for each sample. The scanning rate was 1°/min for this set of experiments.

High energy in-situ heating XRD (HEXRD) experiments were conducted at BL04-MSPD beamline (see Figure 3.4) of ALBA Synchrotron Light Laboratory (see Figure 3.5). Samples were heated up to 773 K with a heating rate of 10 K/min and

diffraction patterns were collected. Alloys were inserted into 1 mm diameter, borosilicate capillaries with low X-ray absorption and sealed in Ar. The wavelength used in these experiments was 0.4962 Å. Wavelength was selected by a double Si monochromator. The data at room temperature was collected free-standing samples. The incoming beam hit the sample surface inclined with 45°. Data were collected in the 2θ range of 0-20°, where θ is the Bragg's angle, using a Mythen array detector system at transmission mode. Samples were not rotated during the experiment.

Figure 3.4 BL04-MSPD beamline in ALBA Synchrotron Radiation Light Source.

Figure 3.5 Photograph of ALBA Synchrotron Light Source.

CHAPTER 4

RESULTS AND DISCUSSION

4.1 Preliminary Investigation of Mn-Al Alloys

This section is an introduction to Mn-Al system regarding the determination of magnetic composition range and kinetic analyses.

4.1.1 Characterization of Alloys in a Certain Composition Range

The boundaries of metastable τ-phase region and high-temperature ε-phase region can be seen on the Al-Mn phase diagram (Figure 2.6). It is clear that there is a certain range of composition (approximately between 66 and 75 wt% Mn) where the metastable magnetic phase can be obtained. The room temperature ranges are not indicated in this phase diagram. Therefore, a broader range of composition was scanned in order to find a composition with τ phase forming ability. Three alloys were produced between 63.8 wt% and 73.0 wt% Mn. The compositions were selected to create significant differences in the compositions such that the far ends of the epsilon and the magnetic range can be investigated. The compositions of these alloys are given in Table 4.1. Alloys are coded as P1 (63.8 wt% Mn), P2 (68.5 wt% Mn) and P3 (73.0 wt% Mn). One problem with these compositions was that an average was taken from many points of the sample. There might have been some deviations from the real compositions since the EDS analysis is performed right after the production.

Table 4.1 Compositions determined by EDS of as-produced samples.

Sample Name	Mn		Al	
	wt%	at%	wt%	at%
P1	63.8 ± 0.1	46.4 ± 0.1	36.2 ± 0.1	53.6 ± 0.1
P2	68.5 ± 0.4	51.6 ± 0.4	31.5 ± 0.4	48.4 ± 0.4
P3	73.0 ± 0.2	57.0 ± 0.2	27.0 ± 0.2	43.0 ± 0.2

After the production and composition determination, the vibrating sample magnetometer (VSM) analysis was conducted for these three samples. B-H curves for these samples were obtained. Figure 4.1 shows the hysteresis curves for these samples. At a first glance, P2 could be referred as a ferromagnetic sample. P3, on the other hand, was definitely paramagnetic. P1 showed a very small magnetic behavior but it was not significant and it could be considered as paramagnetic.

The magnetic behavior right after the production was not expected for these specimens. Specimens should have gained their ferromagnetic behavior after necessary heat treatments at certain temperatures. It was asserted by J. Becker (1968) that upon cooling the sample at a rate of 30 K/s, hexagonal ε-phase transforms into tetragonal τ-phase around 700 °C (973 K) which might have been the cause of the unexpected magnetic properties [14]. This may have been possible during production since the alloys reached up to 3500 °C (3723 K) in the arc melting chamber. Therefore, after melting, the ε-phase may have been formed upon solidification and afterward, some τ-phase formation occurred. This could be the reason of the magnetic properties obtained in Table 4.2. 2025 Oe coercivity and 13.8 emu/g remanence are quite appreciable values for a sample which was not heat treated. P3 seems to be in the range of both ε-phase and τ-phase, however, there was no sign of magnetism for this sample. On the opposite, P1 was not within the region of these phases but it showed some

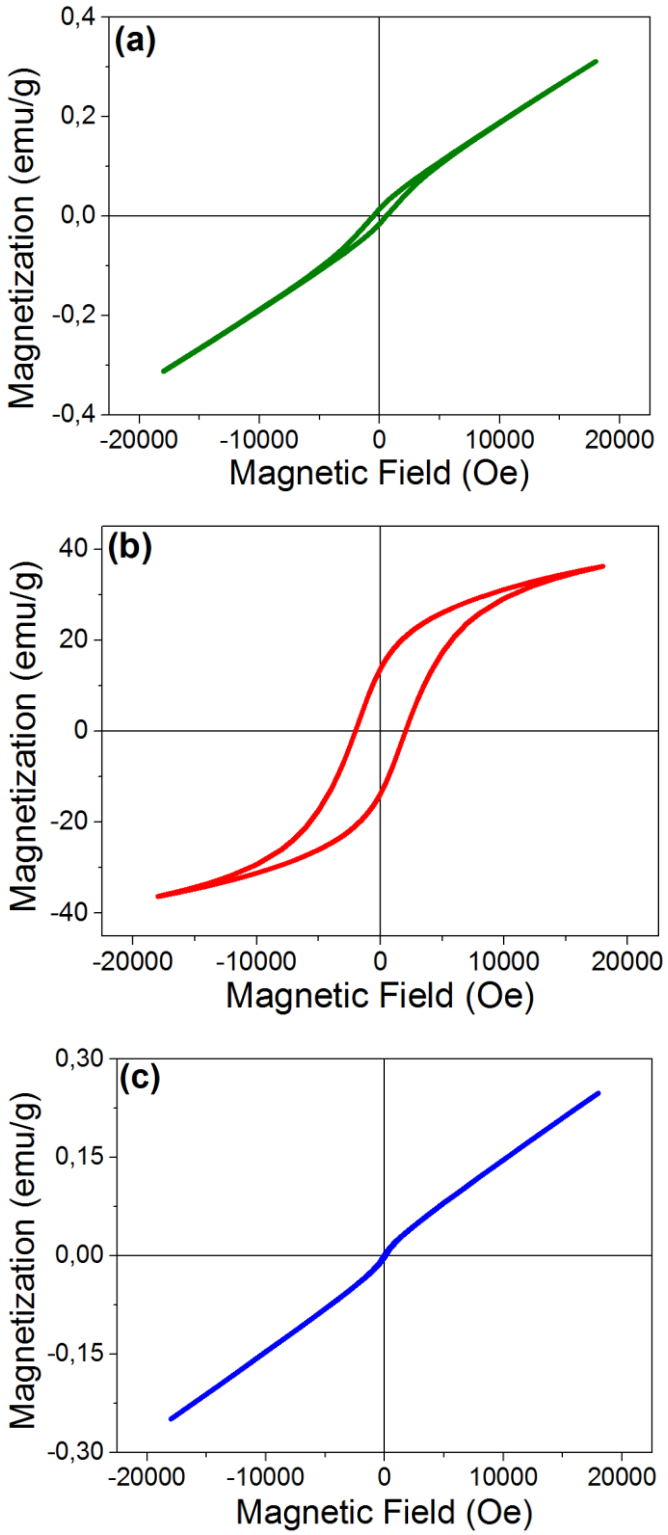

Figure 4.1 Hysteresis curves of (a) P1, (b) P2, and (c) P3 alloys respectively.

coercivity with insignificant magnetization values. It may have been considered as non-magnetic but another sample, results of which were not given here, showed higher magnetic properties with an approximate of 1 wt% higher manganese content. It may also have been due to compositional differences observed. Hence, this alloy system seems to have an optimum range for τ-phase formation which may be around 67 - 72 wt% manganese.

Table 4.2 Magnetic properties of samples P1, P2 and P3.

Sample Name	P1	P2	P3
H_c (Oe)	525	2025	83
B_r (emu/g)	0.015	13.778	0.002
B_s (emu/g)	0.312	36.290	0.249

Figure 4.2 shows SEM images of samples P1, P2, and P3. They were in correlation with VSM results. Clearly, there was no sign of τ-phase in alloys P1 and P3. There could have been some due to the noticeable coercivity of P1, however, they may have been small in size, or they may not exist which could be understood when XRD patterns were examined. P3 was a paramagnetic sample, thus 73 wt% manganese bal. wt% aluminum alloy did not show any magnetic behavior which could be confirmed from SEM micrograph. On the micrograph of P2, the plate-like features could be seen. Those features were signs of τ-MnAl phase. It was in good agreement with the VSM results obtained.

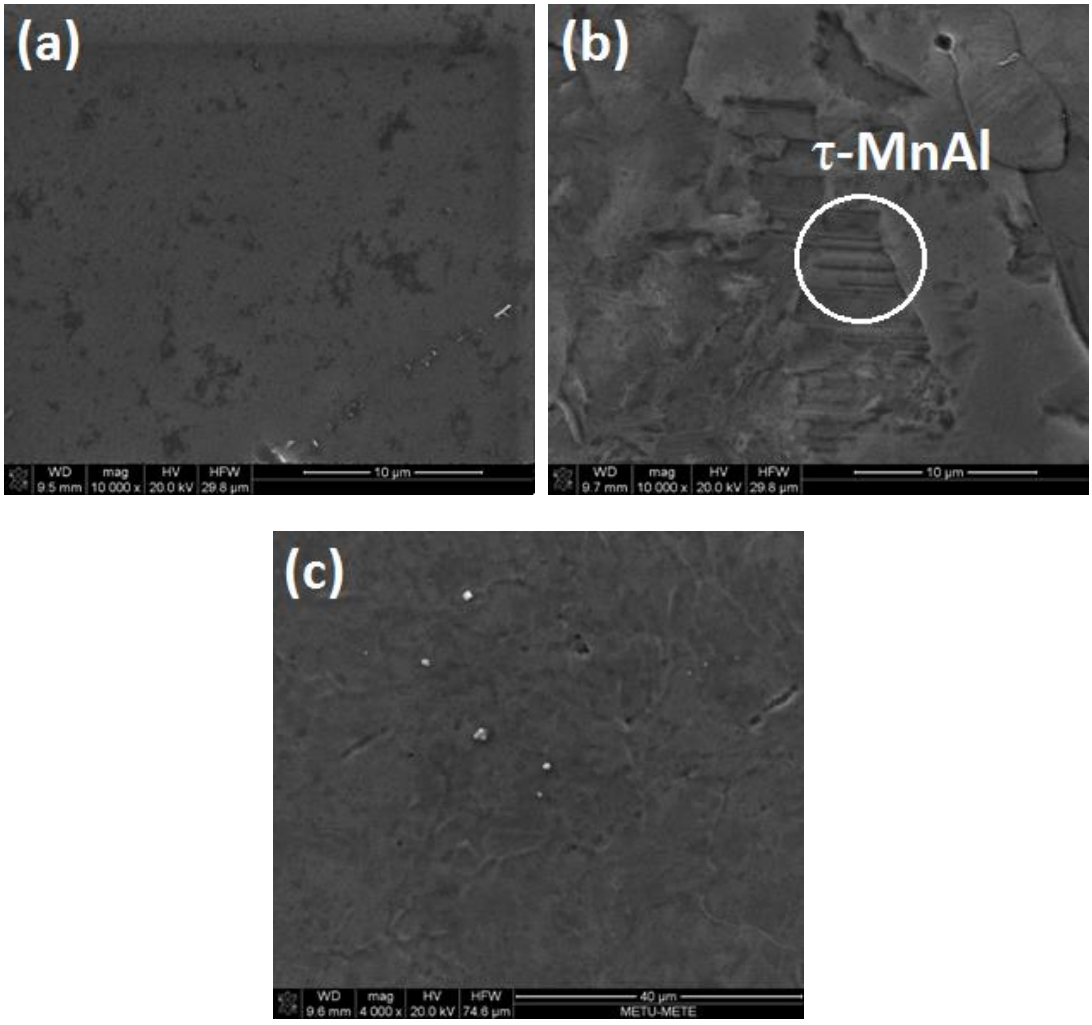

Figure 4.2 SEM micrographs of (a) P1, (b) P2 and (c) P3 alloys respectively.

Figure 4.3 shows the corresponding XRD patterns for P1, P2, and P3 specimens. When these patterns were investigated, it could be seen that there was a small sign of τ-phase for sample P1. This may be the reason for that small coercivity but it was still invisible in SEM. Further TEM analysis was required to detect those under electron microscope. It was expected that almost all of the sample consists of stable phases, mostly γ_2 phase since it was in the composition range of γ_2 single phase region. It could be possible that τ-phase region may be broader at room temperature but it cannot be formed as easily as it was formed at 68 - 71 wt% manganese region. For P2, it was obvious that

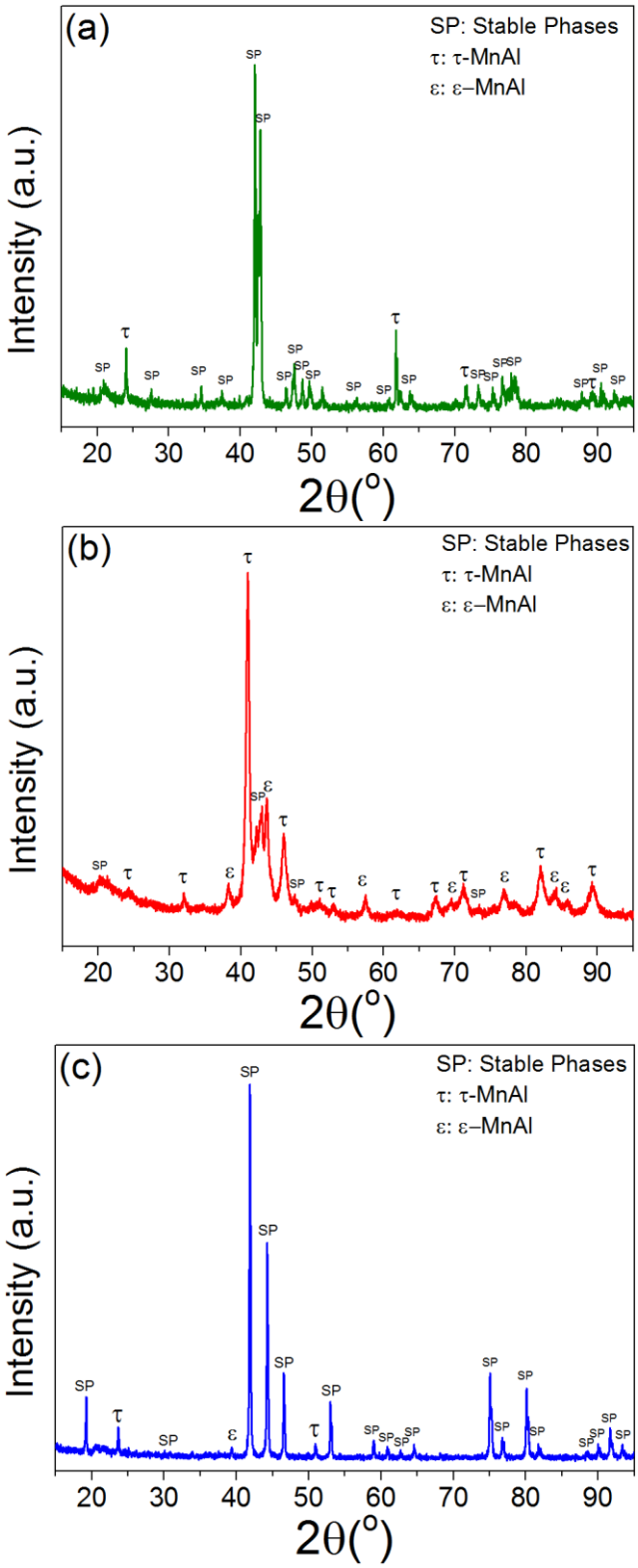

Figure 4.3 XRD patterns of (a) P1, (b) P2, and (c) P3 alloys.

most of the peaks were of τ-MnAl. It was in good agreement with both VSM and SEM analyses. The composition was also clearly in the region of both ε-MnAl and τ-MnAl. During solidification of the alloys, it was expected that first epsilon phase was formed (ε + γ phase region). After that, as noted previously, τ-phase should have been transformed from ε-phase. However, during rapid solidification, while most of the ε phase has transformed to τ-phase, some untransformed ε-phase remained. Moreover, due to the fast kinetics requirement in rapid solidification, the sample could not be totally transformed to either ε-phase or τ-phase. There was clear some evidence of stable phases. For P3 alloy, there was not an observation of magnetic behavior in VSM and SEM analyses. As it could be seen, most of the sample consists of stable phases.

In the literature, the hypothetical τ phase region is shown in Figure 4.4 [40]. These results show that the regions of the phase diagram might be slightly different and these regions should be investigated and determined more precisely.

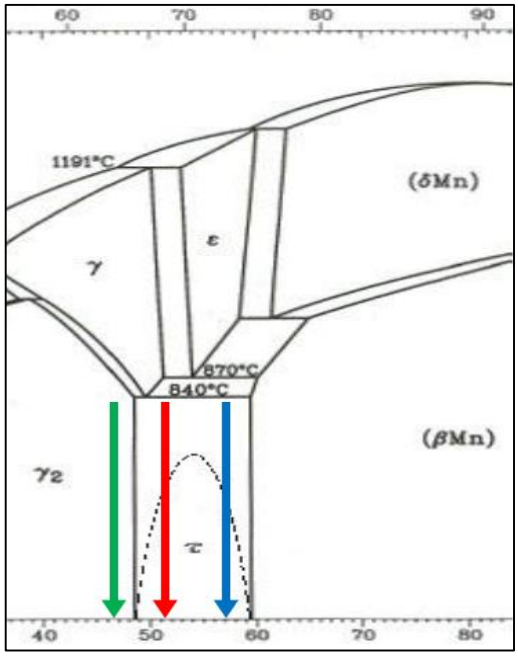

Figure 4.4 Part of Al-Mn Phase Diagram adapted from [40]. Upper scale is wt% Mn and lower scale is at% Mn. Alloys are indicated with green arrow (on left) is for P1, red arrow (in the middle) is for P2, and blue arrow (on right) is for P3.

4.1.2 Kinetic Analyses and Preliminary HEXRD Experiments

After the general characterization of Mn-Al system and alloys in a definite composition range, some kinetic and structural analysis were done for obtaining further information related to the system. A binary alloy was produced with a composition of 70 wt% Mn. It was in the range of desired phases, and it was possible to obtain a ferromagnetic alloy with this composition range. This alloy was named as A1. After the production in arc-melting, it was solutionized at 1150 °C (1423 K) and a single ε phase was obtained. Then, in order to investigate and reveal the phase transformations, in-situ heating high-energy XRD experiment was conducted for this sample in ALBA Synchrotron facility. The phase changes were observed by acquiring XRD patterns, as the sample is heated up to 505 °C (778 K) with a rate of 10 °C/min. After collection of data, 2D film and the 3D representation were constructed (Figure 4.5 and Figure 4.6). It can be easily revealed that first phase transformation occurs at around 380 °C (653 K). It was suspected to be the τ phase. As it occurs, ε phase peaks start to diminish. Then, some other peaks start to appear. For further investigation, XRD patterns collected during isochronal heating should be investigated. Initially, confirmation of room temperature phase was done with high-energy XRD at 32 °C (305 K), then the first phase transformations were observable at 404 °C (677 K), and the final pattern was at 500 °C (773 K). The results coming from the in-situ heating high energy X-ray diffraction (HEXRD) had a wavelength of 0.04134 nm.

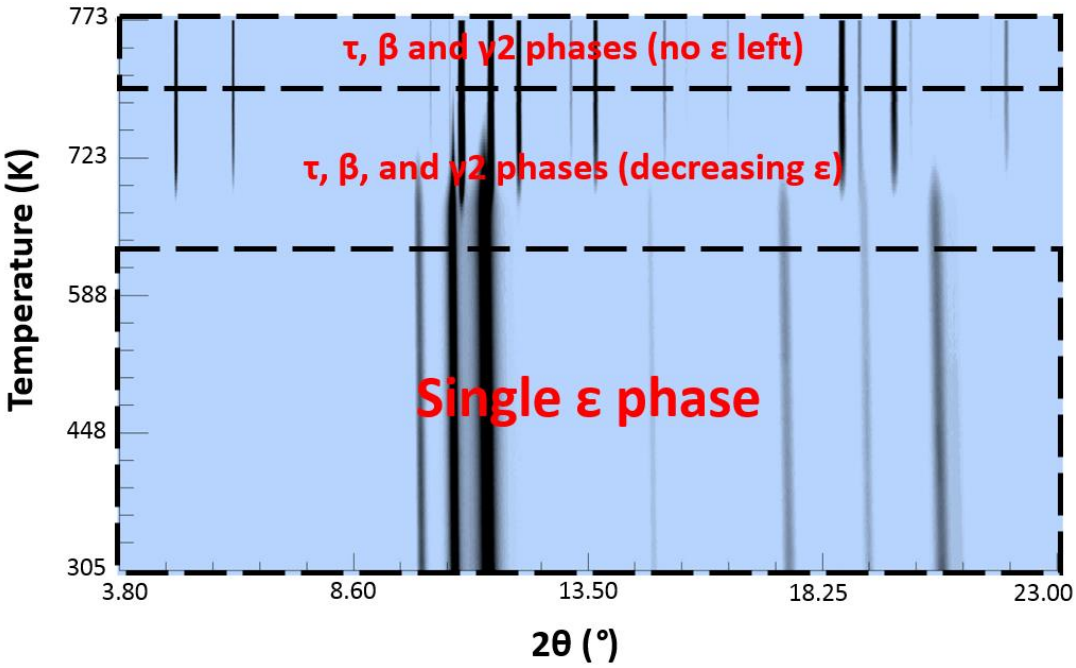

Figure 4.5 2-D film of synchrotron plot of the A1 alloy.

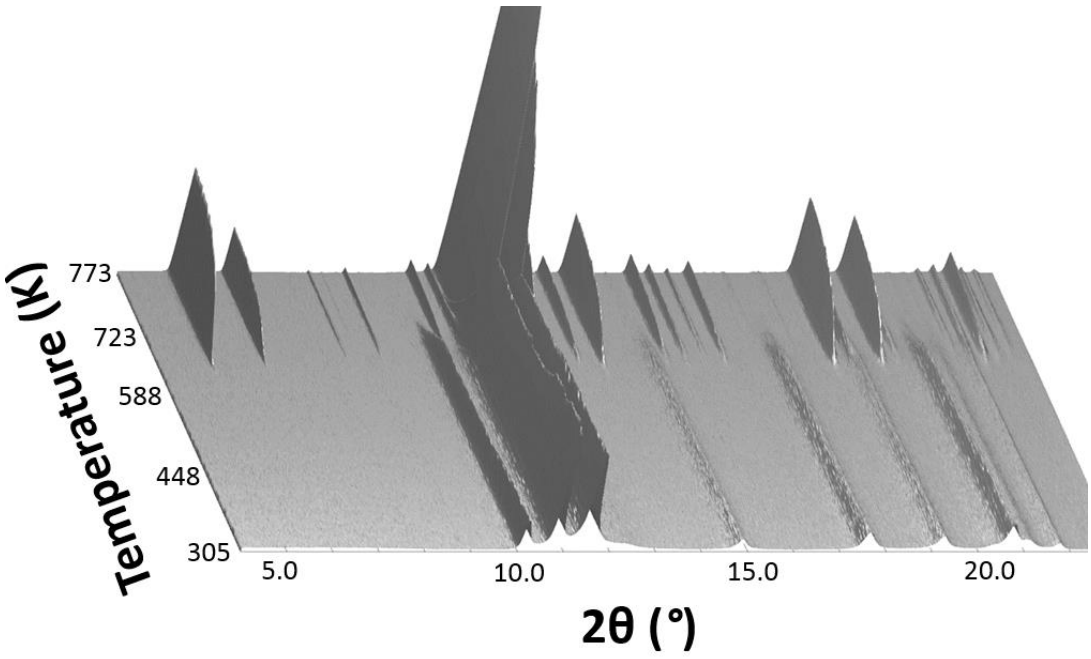

Figure 4.6 3-D representation of synchrotron plot of the A1 alloy.

Figure 4.7 (a), (b), and (c) show the representative 2D XRD patterns collected during in-situ heating. These patterns were given according to Cu-Kα wavelength. The first pattern, 4.7 (a) was observed before the transformation, the second one, 4.7(b) was during the transformation and the third one, 4.7(c) was after the transformation.

The pattern 4.7 (a) at 32 °C (305 K), was a single ε phase pattern as expected after solutionizing. At room temperature, high-temperature ε phase could be trapped through which ferromagnetic τ phase could be formed. Pattern 4.7 (b) 404 °C (677 K) was at a temperature during the transformation, both epsilon and tau phase peaks could be observed as expected. There were also undesired stable phases (β and γ_2) peaks. T phase peaks were growing and the ε phase peaks were diminishing, yet the ε phase peaks were higher in amount which may be a sign of this pattern being at a temperature close to the beginning of transformation temperature and this could be confirmed when the patterns of other temperatures were observed. It took some time for τ phase to form completely and ε phase to vanish. On pattern 4.7 (c) which was at 500 °C (773 K) there was no sign of ε phase since the transformation was completed. As expected most of the peaks were of τ phase and there were some stable phases (β and γ_2) which were not desired in a ferromagnetic Mn-Al alloy.

Figure 4.8 shows a representative TEM bright-field (BF) image of A1 specimen heated up to 500 °C (773 K) and quenched to room temperature. The specimen initially consisted of paramagnetic ε phase. During the continuous heating, ε phase has partially transformed into τ phase as expected from in-situ HEXRD results. BF image shows the embedded τ phase within the ε phase matrix.

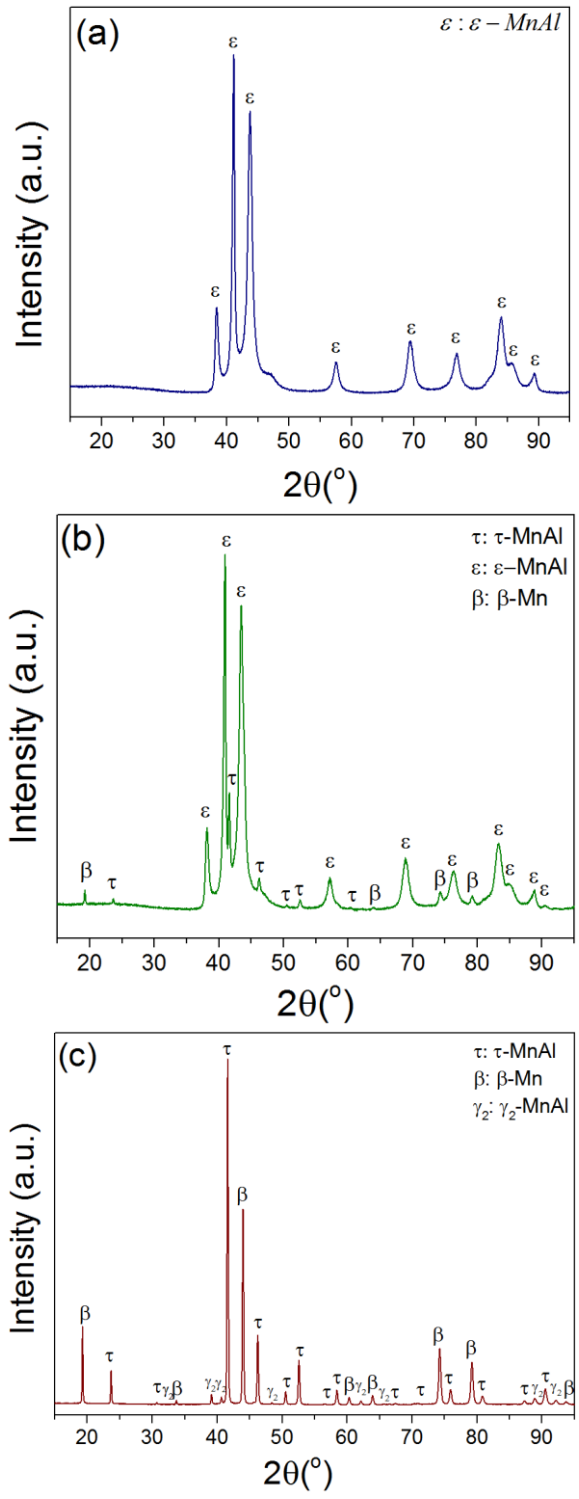

Figure 4.7 Representative in-situ HEXRD patterns of the A1 alloy at (a) 32 °C (305 K), (b) 404 °C (677 K), and (c) 500 °C (773 K), respectively.

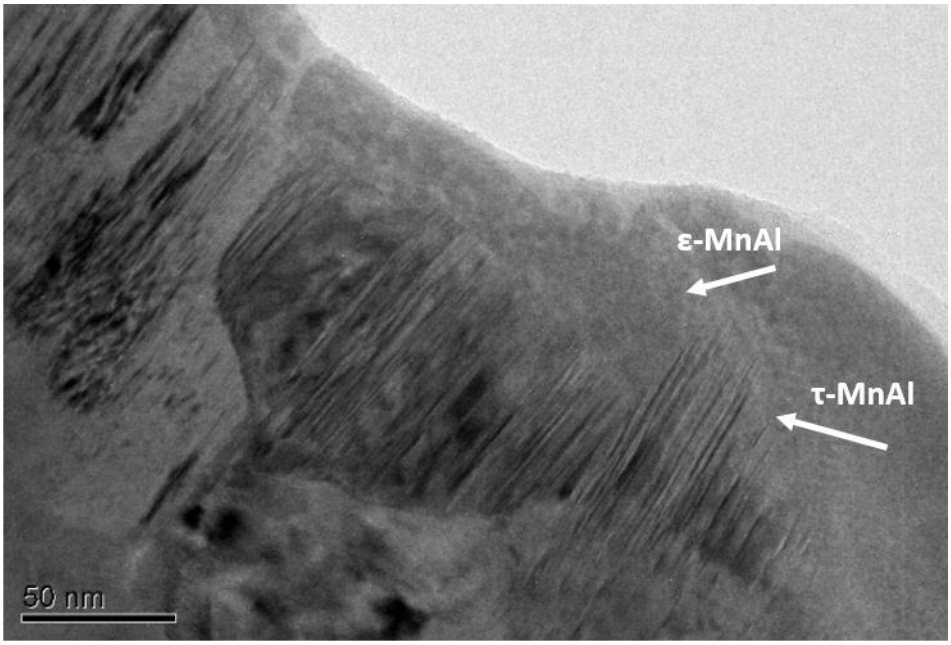

Figure 4.8 Bright Field TEM image of the A1 alloy.

After these investigations, some isochronal kinetic analyses related to Mn-Al system were done in order to reveal the kinetics of the phase transformations within this system. Construction of Kissinger and Ozawa plots was done for two alloys in order to reveal whether the composition alters the activation energy of the phase transformations in the system. These two alloys were named as S1 and S2. S1 has a composition of 67.5 wt.% Mn (50.5 at.%) bal. wt.% Al and S2 had a composition of 70.0 wt.% Mn (53.4 at.%) bal. wt.% Al.

Two alloys were prepared for differential scanning calorimetry for Kissinger and Ozawa analyses. The alloys were heated up to 500 °C (773 K) with four different heating rates which were 10, 20, 30, and 40 °C/min. These DSC traces were plotted in Figure 4.9. Since the τ phase formation started after 350 °C (623 K), only the region including τ phase signal was used for these analyses. It was clear that as the heating rate increases, the peaks were sliding to the higher temperatures. Actually, as it was known from in-situ high-energy XRD experiments, ferromagnetic τ-phase forms first, then the stable phase, β, in that composition range appears. Lastly, stable γ_2 phase

forms. Therefore, in that temperature range, there were three peaks which were convoluted. This caused a problem since the peak temperatures of each phase should be known in order to apply Kissinger and Ozawa analyses. Thus, the DSC traces were fitted to a Gauss function by OriginPro 9.0 software until the fit was converged as it could be seen in Figure 4.10. This fitting operation was reported for all heating rates of both samples. The peak signals for τ, β, and γ_2 phases were clearly observed for each DSC trace. For all heating rates for both samples, critical temperature values were obtained from the fits.

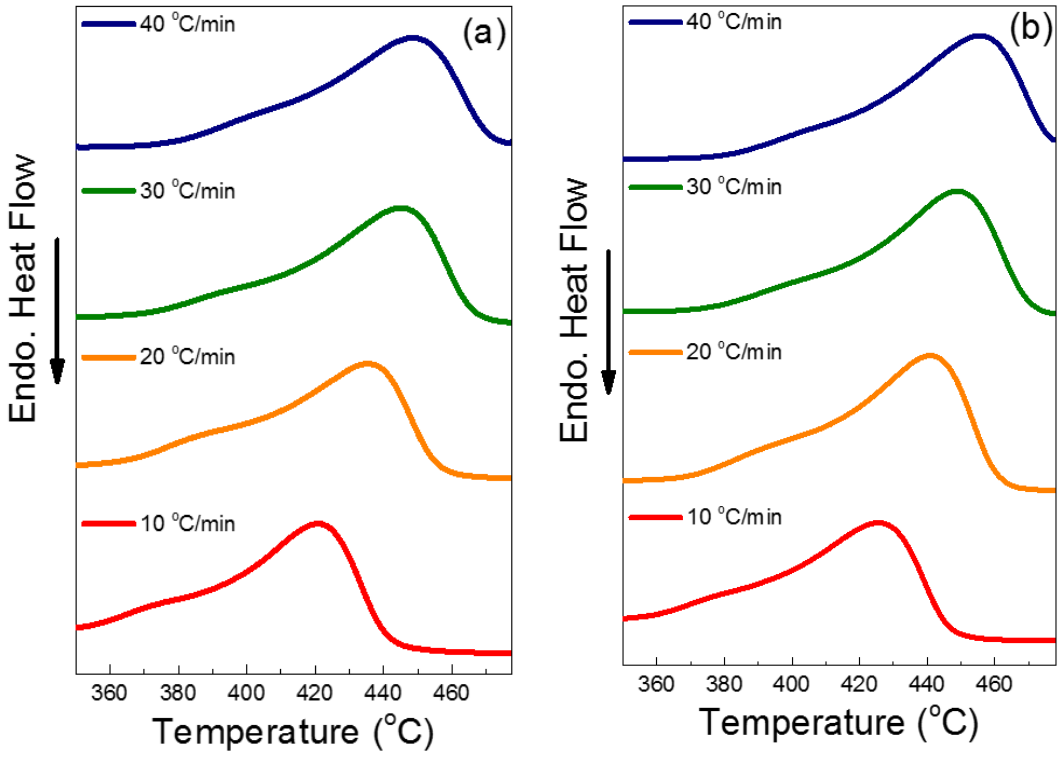

Figure 4.9 DSC curves of alloys (a) S1 and (b) S2 at 10, 20, 30 and 40 °C/min heating rates.

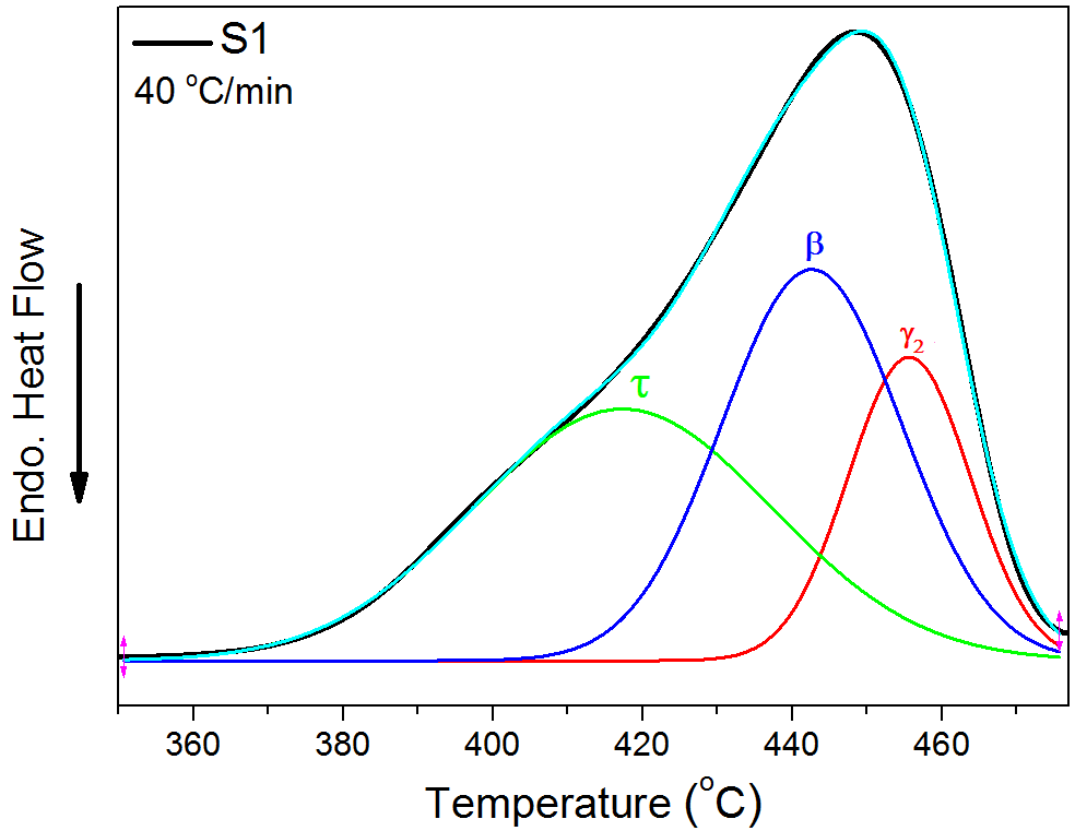

Figure 4.10 Peak fit (Gaussian) done by OriginPro 9.0 software. Representation of phase transformation signals on the DSC trace of sample S1 with a heating rate of 40 °C/min. The black line is original data and the cyan line is the Gaussian fit.

In order to reveal and compare the activation energy of magnetic τ phase formation upon heat-treatment, Kissinger, and Ozawa plots were constructed. The background information was given in literature review chapter. Basically, for the Kissinger plots, $\ln(\phi/T_p^2)$ vs. $1000/T_p$ was constructed where ϕ is the heating rate and T_p was the peak temperature. For the Ozawa plot, it was similar but the plots of $\ln(\phi)$ vs. $1000/T_p$ were obtained. These plots could be seen in Figure 4.11 for both samples. Plots (a), (c), and (e) were the Kissinger plots for τ phase, β phase, and γ_2 phase, respectively. Also, plots (b), (d), and (f) were the Ozawa plots for τ phase, β phase, and γ_2 phase, respectively. In each case, both S1 and S2 plots were given separately.

After the plots were drawn, linear fits were applied for each plot to calculate the activation energies. These were plotted with an x-axis of $1000/T_p$ in order to obtain the activation energy values in units of kJ/mol. After multiplying the related values with gas constant, R, the activation energies were obtained both with Ozawa and Kissinger methods for each phase for both alloys. These values are tabulated in Table 4.3.

Slopes of Ozawa plots were different than Kissinger plots but since the formulas used for each are different, they came out to be pretty similar. When the activation energy values were investigated in detailed, there is not a remarkable difference between the values of sample S1 and S2. The difference in values was always equal or less than 4 kJ/mol which was less than 1% for all calculations. This was a reasonable difference which may even be due to errors in fitting and calculations. Thus it could be derived that composition does not change the activation energy and this energy value was approximately 140 kJ/mol for τ phase formation. For β phase, the value was higher than the value for τ phase which was 168 kJ/mol in average. The γ_2 phase had an activation energy average of 179 kJ/mol which was the highest value. There were not too many studies related to kinetics and activation energy of τ phase formation. One example could be given from the literature. Yanar et al. (2002) were plotted an Arrhenius plot in order to experimentally find the diffusional growth activation energy for Mn-Al alloys. Thus, due to experimental growth kinetics, they calculated an activation energy of ~154.4 kJ/mol [38]. There was less than 10% difference between the values calculated here and the values they obtained.

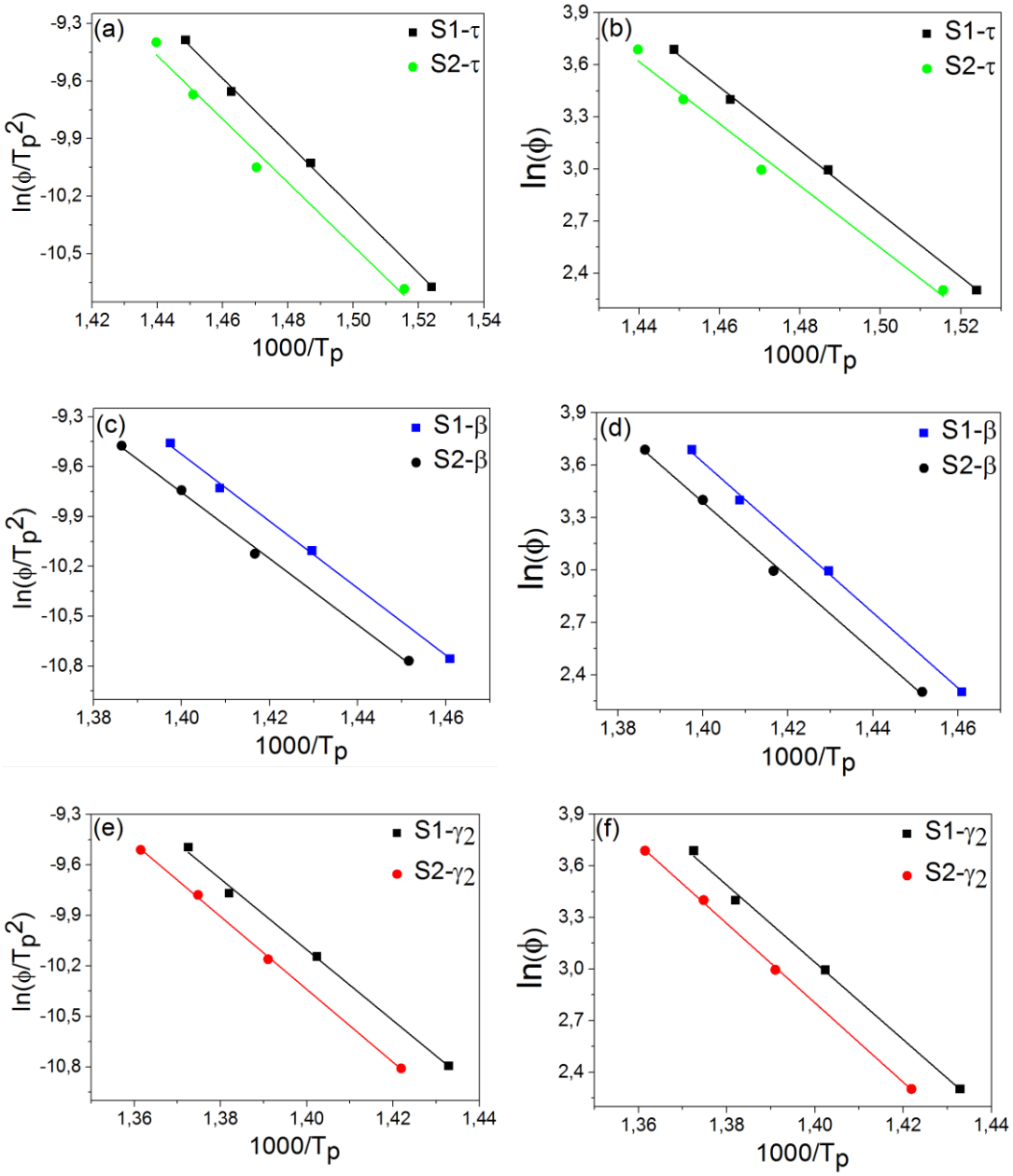

Figure 4.11 Kissinger plots for (a) τ phase of samples S1 and S2, (c) β phase of samples S1 and S2, (e) γ_2 phase of samples S1 and S2, and Ozawa plots for (b) τ phase of samples S1 and S2, (d) β phase of samples S1 and S2, (f) γ_2 phase of samples S1 and S2.

Table 4.3 Calculated activation energies for the phase transformations of alloys S1 and S2 by Kissinger and Ozawa analyses.

Phase	Kissinger E_c (kJ/mol)		Ozawa E_c (kJ/mol)	
	S1	S2	S1	S2
τ-MnAl	140	137	144	141
β-Mn	167	166	170	169
γ_2	175	180	178	182

The effect of composition seemed to be insignificant in terms of the activation energy required to form the ferromagnetic τ phase. On the other hand, the composition of binary Mn-Al was quite crucial to designate the thermodynamical behavior of the metastable and stable phases upon continuous heating. Therefore, a more detailed in-situ HEXRD analysis was done according to composition change and results were given in the next part. The composition seemed to affect the phase transformations, thus the phases forming in the alloy, the magnetic properties and the structure of the material. In the next chapter, effect of composition on the phase transformation hierarchy is discussed in details.

4.2 Effect of Composition on the Phase Transformations in Mn-Al system

After the first section, where composition seemed to be an important issue, and it was understood that phase transformations should be investigated in more detail, four other alloys with various compositions were produced by arc-melting. The compositions were selected according to the possible τ phase forming region on the phase diagram [41]. After production, all samples were solutionized to obtain paramagnetic ε phase. The samples were coded as S1, S2, S3, and S4 for simplicity and the composition of each sample, verified by EDS analysis, and given in Table 4.4.

Table 4.4 EDS results of the samples S1, S2, S3, and S4. Mn and Al ratios of the alloys are given in both atomic and weight percentages.

Sample Name	Mn		Al	
	wt%	at%	wt%	at%
S1	67.5 ± 0.3	50.5 ± 0.3	32.5 ± 0.3	49.5 ± 0.3
S2	70.0 ± 0.2	53.4 ± 0.2	30.0 ± 0.2	46.6 ± 0.2
S3	71.5 ± 0.1	55.2 ± 0.1	28.5 ± 0.1	44.8 ± 0.1
S4	73.0 ± 0.5	57.0 ± 0.5	27.0 ± 0.5	43.0 ± 0.5

The solutionizing parameters were the same as before, the alloys were held at 1150 °C (1423 K) for an hour. Then they were water quenched. Solutionizing was performed under atmospheric conditions. Samples were confirmed to be single ε-phase with XRD analysis. The after-solutionizing XRD patterns are given in Figure 4.12. These patterns possessed single ε phase only and they were similar for all of the samples. These were also confirmed with HEXRD.

After solutionizing, and confirmation of single ε-phase for all samples, they were annealed up to 500 °C (773 K) with a heating rate of 10 K/min in DSC and rapidly solidified to room temperature. The heating curves obtained in DSC are given in Figure 4.13. When the heating curves were examined, it could be seen that there is the difference in the signals between S1, S2, and S3, S4. For S1 and S2, it was observed that they had a small hump at around 247 °C (520 K) followed by a peak at around 377 °C (650 K). That hump that was seen on S1 and S2 is suspected to be the formation of ε'-phase. Alloys S1 and S2 had two convoluted peaks leaned towards right. The first one may be a possible τ-phase formation and the second peak may be related to stable phase formation. On the other hand, the heating path of the alloys S3 and S4 had a single peak leaned towards left at around 347 °C (680 K). There was not a similar hump as in S1 and S2. The peak for S3 and S4 might be an overlap of τ-MnAl and

stable phase formation signals. Onset temperature of the peak in S1, S2, S3, and S4 were calculated as 364 °C (637 K), 363 °C (636 K), 354 °C (627 K), and 348 °C (621 K), respectively. There seemed to be an effect of composition on the shape of the curve which could be observed in the heating patterns (Figure 4.13).

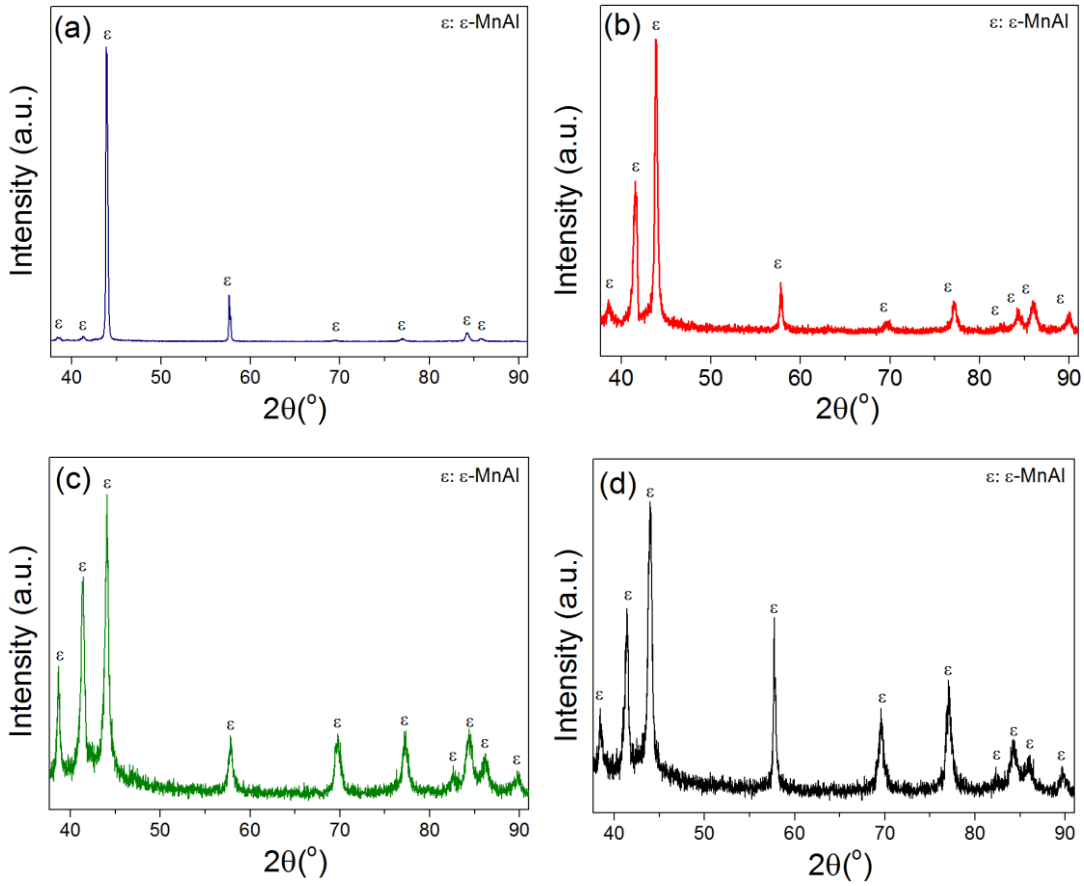

Figure 4.12 XRD pattern of sample (a) S1, (b) S2, (c) S3, and (d) S4 after solutionizing.

In order to further observe and understood this enigmatic behavior in Mn-Al system, these alloys were prepared for in-situ heating high-energy XRD analysis (HEXRD). In-situ heating synchrotron analysis was carried out on these samples for the identification of the signals observed in DSC and investigate the transformation kinetics and hierarchy. A similar experimental procedure was adapted for comparison

and correlation with DSC data. As-solutionized specimens of alloys S1, S2, S3, and S4 were also used in the conduction of in-situ heating HEXRD analysis which had single ε-phase. Alloys were again heated up to 500 °C (773 K) with a heating rate of 10 K/min within a furnace attracted to the synchrotron beamline. During this process, simultaneous XRD patterns were obtained with a wavelength of 0.4962 Å. 2-D films with temperature vs. 2-theta axes were constructed which can be seen in Figure 4.14. The purpose of this procedure was to mimic the DSC patterns as shown above. Therefore, it has been possible to observe phase changes and understand the transformations occurring during the process.

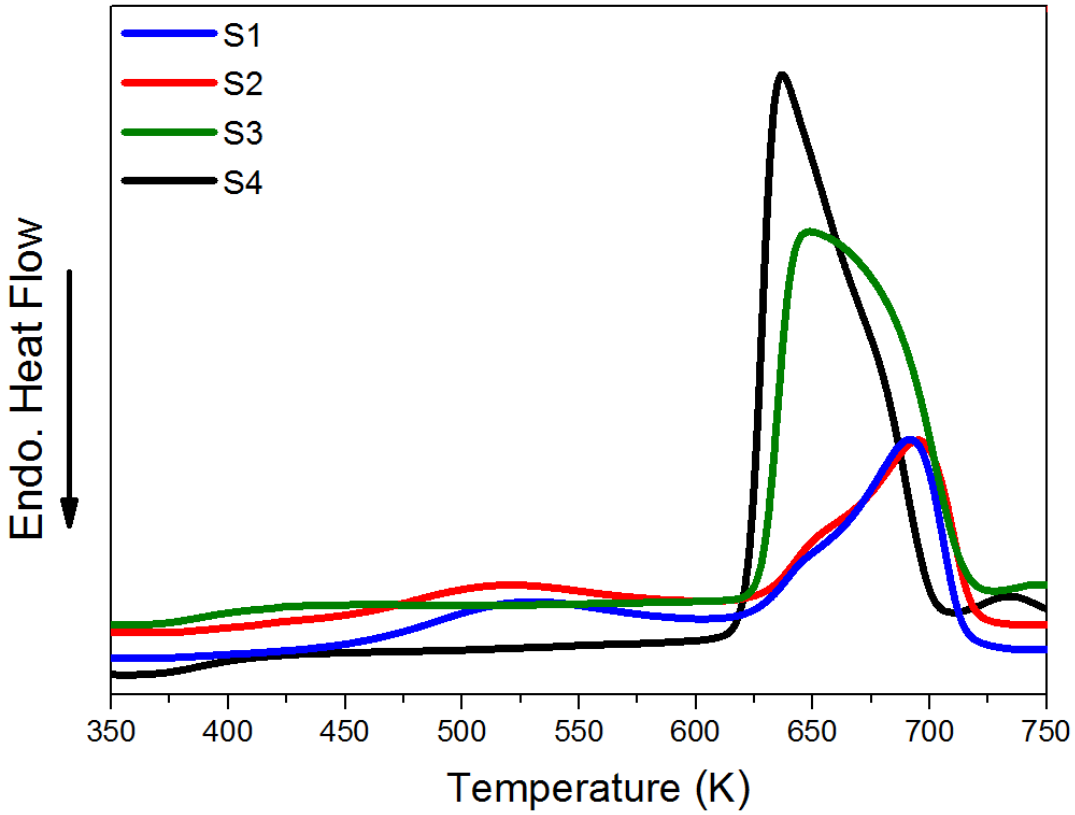

Figure 4.13 DSC heating curves of S1, S2, S3, and S4 with 10 K/min from room temperature to 773 K.

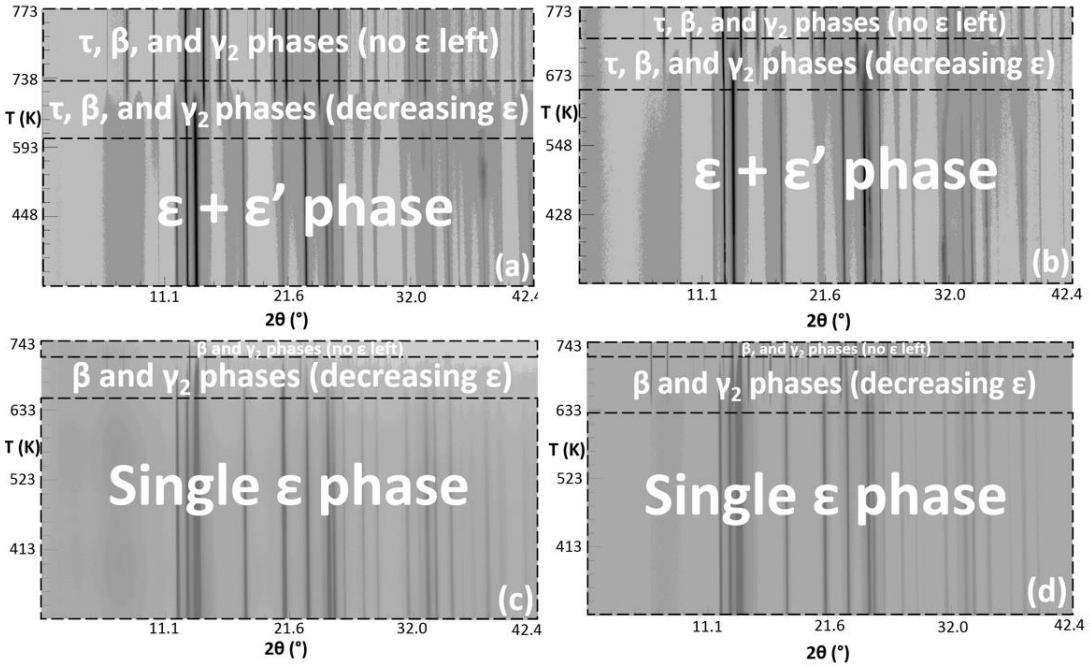

Figure 4.14 2-D film synchrotron plots of (a) S1 (b) S2, (c) S3, and (d) S4.

When these 2-D films were analyzed, it could be seen that they are very similar to DSC scans, the heating path differs for alloys with less Mn (S1 and S2) and for the alloys with larger amounts of Mn (S3 and S4). A broad peak with low intensity was present around 9° (2θ) in S1 and S2 whereas that signal was missing for the alloys S3 and S4. This peak can be seen in Figure 4.14. It looked like a very distinct shadow on the 2-D plots of samples S1 and S2. For samples S3 and S4, there might be that signal, there was a small contrast on the films and this range should be investigated closer.

ε and ε' phase have overlapping diffraction patterns and the peak at 8.9° (2θ) is characteristic only for the orthorhombic ε' phase. ε' is an intermediate phase and is not shown on the phase diagram. Due to its low intensity at small 2θ angles, presence of ε' is hard to distinguish without the use of in-situ heating high energy X-ray diffraction. This finding was in good correlation with the DSC scans showing a similar signal prior to the ε-to-τ transformation. It was likely that the hump observed at DSC around 227 °C (500 K) for the S1 and S2 alloys corresponds to the ε→ε' transformation. These

signals seemed to be observable also at room temperature, therefore, they should be observed in more detail, because this peak could be a key for the transformations and might reveal the differences seen in DSC scans. It was also observed that samples S3 and S4 did not contain any τ-phase, whereas samples S1 and S2 had signs of magnetic τ-phase. This may also be related to the ε' peak on samples S1 and S2.

For this purpose, all of the patterns for all samples were examined from 220 °C (493 K) to 470 °C (743 K). With a closer look at the 2θ range of 8.2° - 9.6°, the distinctive ε' peak could be found in Figure 4.15. This figure revealed that the phase transformation sequence was quite similar in S1 and S2 but it shows some differences for S3 and S4. In the case of S1 and S2, there existed ε' phase at room temperature. Since the patterns of ε and ε' were quite similar, the case may even be a single ε' phase. However, the distinct peak of ε' disappeared at a certain temperature. On the figure, it was clear that the existing ε' phase in sample S1 and S2 slowly increased in intensity, and then suddenly disappeared. In alloy S1, the hump at room temperature around 8.9° (2θ) transformed into a peak at 360 °C (633 K) and vanished at around 451 °C (724 K). In alloy S2, the same pattern was observed but the temperature range changes. ε' peak reached its maximum value at 411 °C (684 K) and disappeared at 469 °C (742 K). For these samples, with diminishing ε and ε' phases, τ phase started to form. As the temperatures increased, ε/ε' to τ phase transformation was followed by the formation of stable non-magnetic phases, β, and γ_2 which was not shown in this figure.

Samples having Mn content higher than 70% by weight (S3 and S4) did not have any peaks at 8.9° (2θ). ε' phase was absent at the quenched state for S3 and S4 alloys. Room temperature ε phase directly transformed into stable β and γ_2 phases with increasing temperature, surpassing the ferromagnetic τ phase transformation. Thereby without the presence of ε', τ phase could not be obtained in alloys S3 and S4 with this heat treatment procedure. It could be said that τ nucleates and grows only from the ε' phase, but stable phases arise from both ε and ε' phases. In correlation with DSC heating curve, the convoluted peaks of S1 and S2 may belong to τ-phase and stable

phases respectively. The single peak of S3 and S4 probably corresponds to the formation of the stable phases. The change in transformation scheme indicates the significance of the ε' phase in terms of τ-phase formation. It is likely that ε' phase serves as a nucleation site for τ-phase formation. During the heating process, the peaks of metastable τ-phase appear with increasing temperature which was not shown in Figure 4.15. ε and ε' matrix completely diminished after 740 K for alloys S1 and S2.

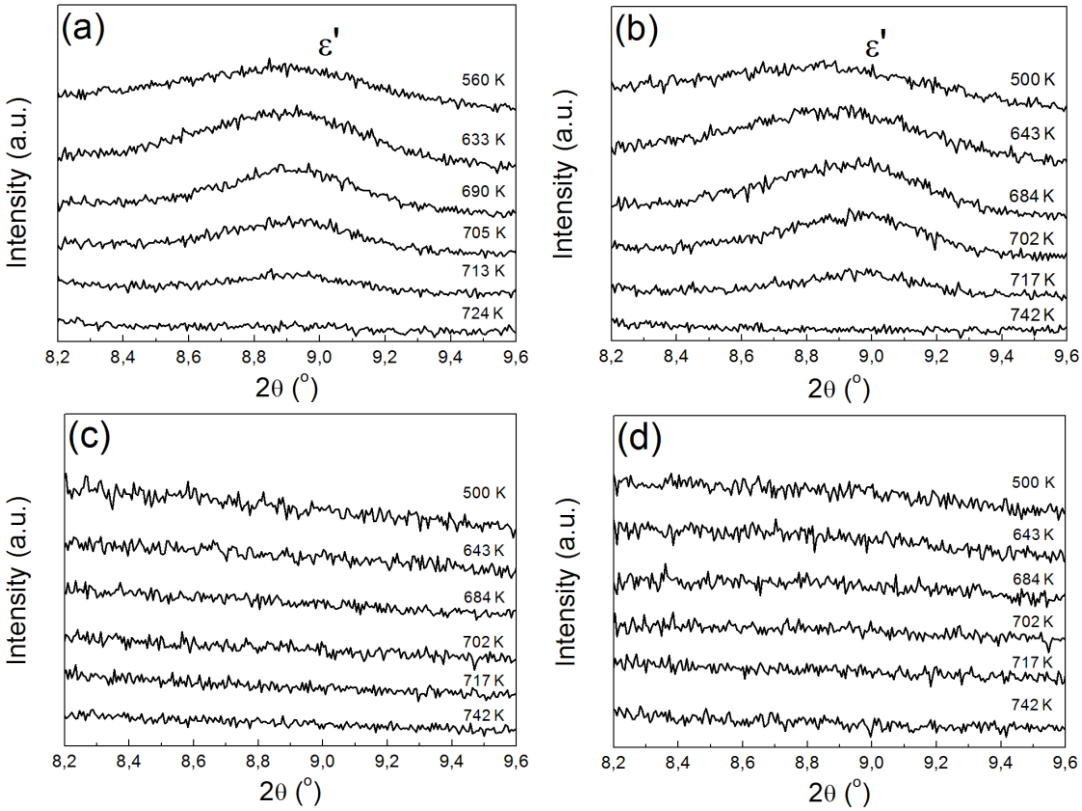

Figure 4.15 ε' peak range at different temperatures for samples (a) S1, (b) S2, (c) S3, and (d) S4.

With this information, it could be said that ε' phase should be present in order τ-phase to be formed. Without the presence of ε' phase such as for samples S3 and S4, the magnetic phase formation was not possible. This small detail could only have been seen by in-situ heating high-energy XRD analysis. Otherwise, the effect of composition on ε' phase and hence τ phase could not have been understood. After a

certain content of manganese, it was not possible to obtain ε' phase. Thus, even they were in the range of ε and τ phases, with those compositions, it was not possible to obtain a ferromagnetic Mn-Al alloy. A reasonable composition range for these alloys could be given that the manganese content should be between 67.5 wt% and 71 wt% Mn. Both of these boundaries could be investigated in more detail for a more precise range of composition. Moreover, the issue behind the formation of τ phase seems to be more obvious with this investigation. For further information, the formation of τ-phase and the formation of the stable phases can be investigated. For understanding the relations of ε' phase, the 2θ range of 8.2° - 9.6° is investigated. The first peak of τ phase and the first peak stable phase form in the 2θ range of 11.5° - 15.0°. They also form at higher temperatures, as ε and ε' phase peaks start to diminish. Therefore, observation of them should be done according to these data.

For this investigation, Figure 4.16 can be used. This figure was at elevated temperatures in order to see the formation of τ phase and the stable phases. The patterns for all samples were examined between 325 °C (598 K) to 470 °C (743 K) in the 2θ range of 11.5° - 15.0°. This figure provided a better understanding related to the phase transformations in the system. As it could be seen in the figure, diffraction patterns for all of the samples were given. In the first four of them (from (a) to (d)), the formation of τ phase was investigated. For the last four (from (e) to (h)) on the other hand, the formation of the stable phases (in this case β-Mn phase) were observed. It has been seen that the transformation sequence and phases transformed changes due to the composition. Thereupon, in relation with this, also the transformation temperatures showed a variety with respect to composition. ε/ε' matrix transforms into τ phase at 360 °C (633 K) and 370 °C (643 K) for S1 and S2 respectively (Figure 4.16a, 4.16b) whereas τ phase peaks were missing for S3 and S4 (Figure 4.16c, 4.16d).

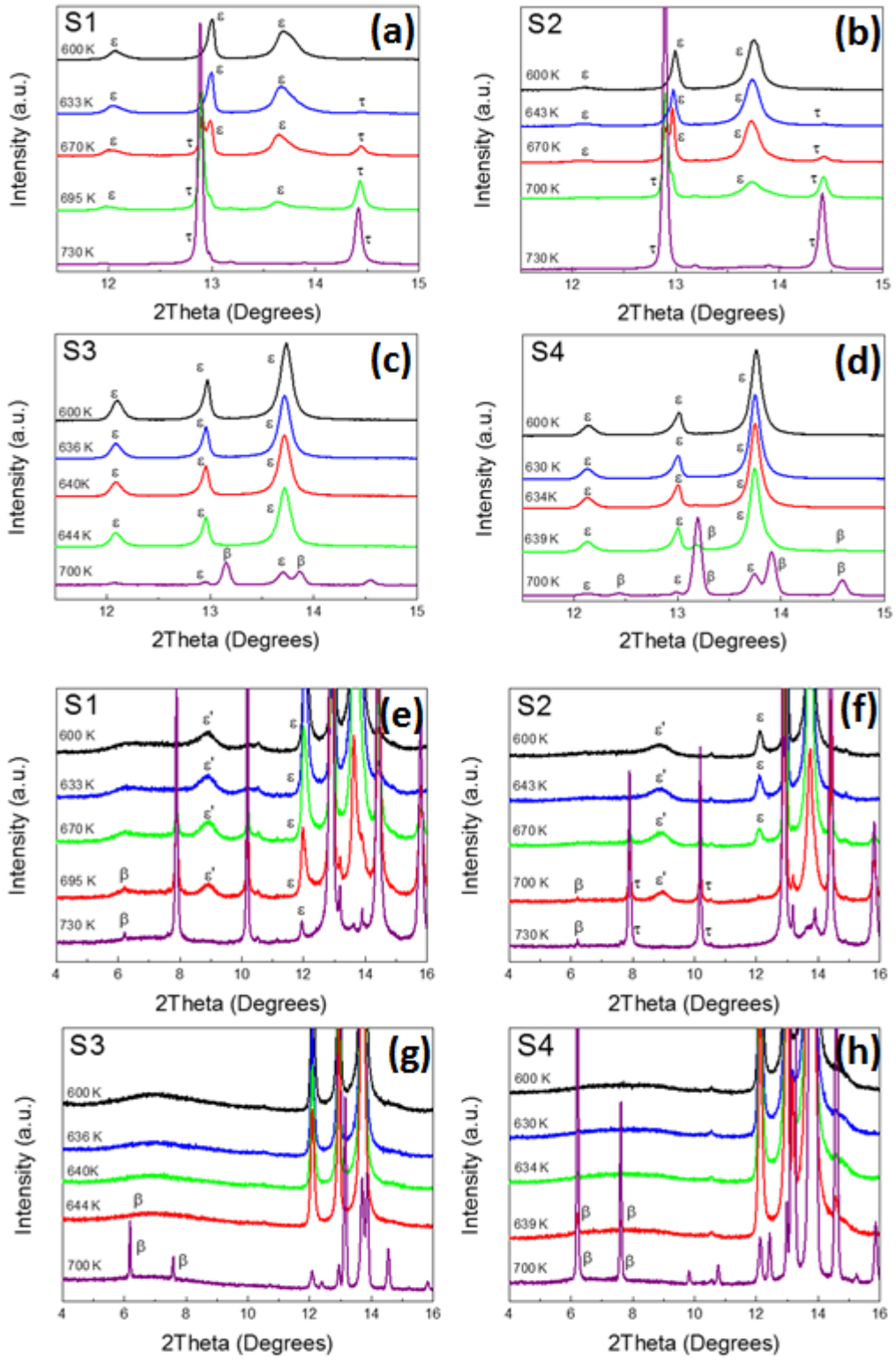

Figure 4.16 The τ-phase and stable phase formation for samples S1, S2, S3, and S4.

They were in good agreement with previous results. It was indicated that τ phase can only be observed for samples containing ε' phase which is clear on this figure. Stable non-magnetic phases, β, and γ_2 are formed subsequently at 422 °C (695 K) and 425 °C (698 K) for S1 and S2, respectively (Figure 4.16e, 4.16f). Hence, there was a difference of 55-60 K between the formation of τ-phase and stable phases (β and γ_2). In the case of S3 and S4, ε phase directly transformed into stable β and γ_2 phases instead of τ phase (Figure 4.16g, 4.16h). Stable phases were formed at 356 °C (629 K) and 357 °C (630 K) for S3 and S4, respectively. Thus, the temperature difference between the τ-phase and stable phases (β and γ_2) lowered down to 5-10 K. This suggests that presence of ε' phase not only promotes the τ-phase formation but also retards the transformation to the stable phases.

All of the critical temperatures mentioned above are listed in Table 4.5. When the samples were compared, it could be seen that the distinct ε' peak diminished just a little bit before the ε phase peaks totally vanished. It could also be said that the temperature where ε' diminished for samples S1 and S2, ε phase diminished for samples S3 and S4. It could also be seen that the increase in τ phase peaks' intensities started when the ε' peaks diminished.

Table 4.5 Ranges of the phases ε, ε', τ, β, and γ_2 for samples S1, S2, S3, and S4.

Sample Name	Phase and Formation Range (K)			
	ε	**ε'**	**τ**	**β, γ_2**
S1	RT-741	463*-726	633-773	695-773
S2	RT-740	479*-731	643-773	698-773
S3	RT-729	-	-	629-773
S4	RT-729	-	-	630-773

*Temperature where ε' peak starts to intensify.

After investigating in-situ high-energy XRD patterns and DSC scans for samples S1, S2, S3, and S4, VSM tests were conducted from these specimens. For these four

samples, hysteresis curves were obtained and the results are given in Figure 4.17. These curves are obtained under 5 Tesla applied magnetic field.

Alloys S1 and S2 showed ferromagnetic behavior as expected due to the presence of τ-phase. Coercivity and remanence of S1 were found to be 640 Oe and 23 emu/g, respectively. S2 had relatively stronger magnetic behavior with the coercivity of 1560 kOe and remanence of 26 emu/g. On the other hand, S3 and S4 were paramagnetic in nature as τ-phase was not observed. Increasing Mn content led to better magnetic properties but up to the composition where there could not be any τ phase obtained. As it was predicted from HEXRD and DSC results, if ε' phase is not present as a precursor, τ phase cannot be formed. This causes a paramagnetic behavior after the corresponding heat-treatment. Therefore, an alloy with 68 – 71 wt% Mn bal. wt% Al seemed to be in the optimum range. A more precise range could be found by characterization of compositions with a narrower range.

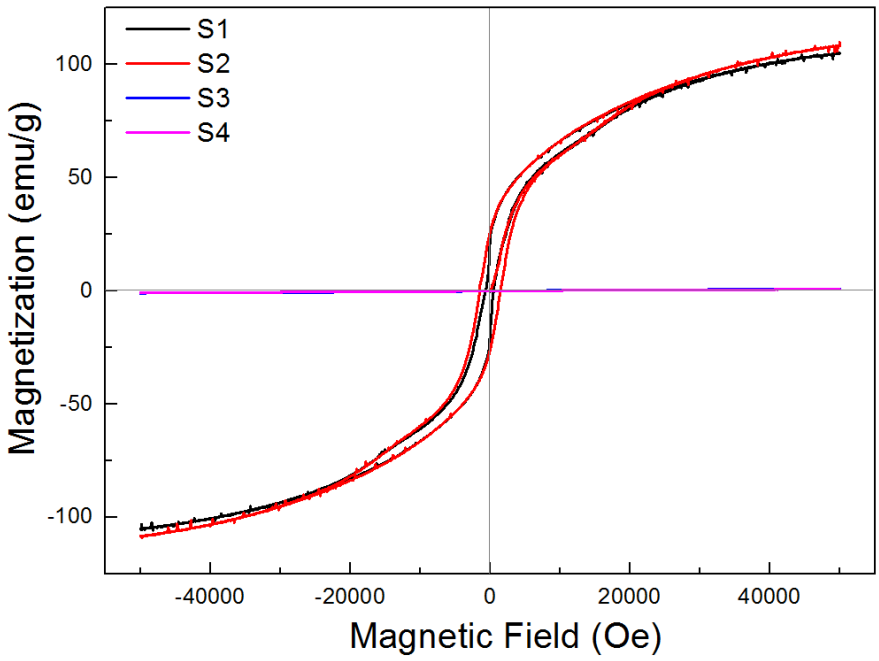

Figure 4.17 Hysteresis curves of samples S1, S2, S3, and S4.

After observation of ferromagnetic τ phase in samples S1 and S2 during in-situ high-energy XRD experiments and on the DSC traces, confirmation was done by vibrating sample magnetometer (VSM). Lastly, in order to reveal the corresponding microstructure, optical microscopy, and SEM analyses were performed. In Figure 4.18, plate-like τ phase features could be observed. Since there was not any ferromagnetic behavior for samples S3 and S4, their images are not shown here.

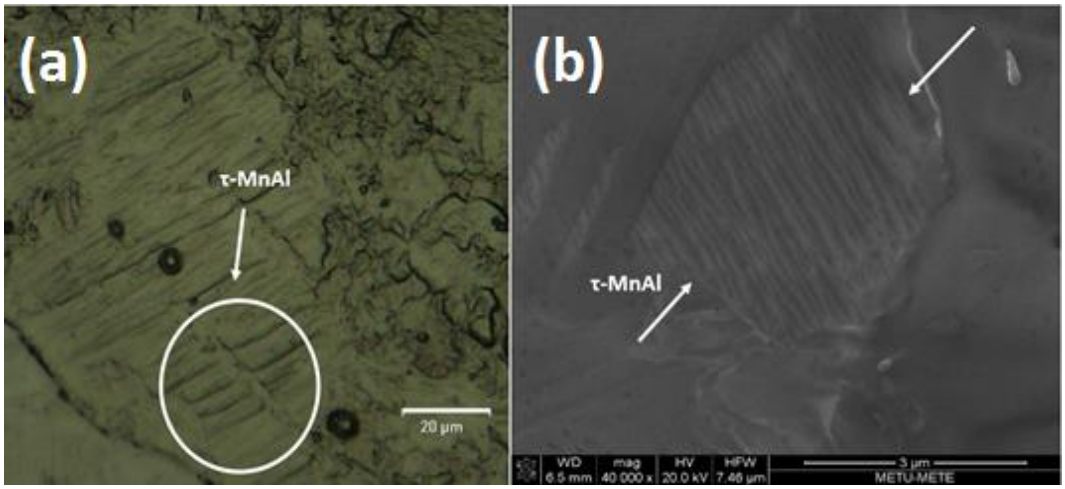

Figure 4.18 (a) Optic microscope image and (b) SEM image of alloy S2. On the optical microscope image, some of the τ phase is indicated with arrows.

To sum up these results, it could be said that composition has a significant effect on the formation of ferromagnetic τ phase since it affects the transformation sequence, phases present, and their formation temperature. The transformation from ε phase to τ phase may occur in several ways. When the current literature is considered, the transformation occurs by massive transformation, by shear mode or their combination. To stabilize the τ phase, addition of C is also common. Thus, when the alloy has higher amounts of manganese and carbon, the shear mode of transformation is more dominant by the formation of ε' phase. However, when the amount of manganese and carbon becomes less, massive transformation path is observed [85-87]. However, these results show that a phase transformation including ε' phase occurs when the manganese

content is not as high as 71.5 wt%. As the manganese content becomes higher, neither ε' phase nor τ phase is observable. The ε phase is not useful by itself and only the stable phases can be observed. Moreover, when the Mn content decreases, stable phases form at higher temperatures. Thus, in order to form τ phase, an alloy must present ε' phase during the transformation or else only the stable phases form. Hence, an increase in the amount of ε' phase may mean a higher amount of τ phase, which may lead to higher magnetic properties for this alloy. Thus, the optimum composition should be determined with a more precise investigation and heat treatment parameters. For determination of the predominant transformation mode, the morphology of the phases, their sizes and transformation should be carefully understood. Analyses with advanced electron microscopy techniques could be helpful in this situation. It should be noted that in-situ heating synchrotron analyses are carried out during isochronal heating. For a complete understanding, isothermal annealing should also be incorporated.

CHAPTER 5

CONCLUSION AND FUTURE RECOMMENDATIONS

5.1 Conclusion

The main purpose of investigating Mn-Al alloys was to obtain a RE-free permanent magnet which could be used particularly in common magnetic applications. However, this alloy system should be investigated and improved before it becomes available for conventional use as a credible permanent magnet. In this study, the main focus was to investigate the effect of composition on the kinetics of these alloys and the phase transformations occurring in the system. Therefore, in-situ high energy X-ray diffraction techniques were pretty supportive. Moreover, a general understanding of the system was gained.

First of all, the general investigation of the Mn-Al alloys was conducted. During this process, it was found that composition had an important impact on the magnetic properties and the structure of the alloys. However, the composition did not show a significant effect on the activation energy of phase transformations. Rather than the activation energies, the composition was effective on the phase transformations such that there is a certain limit which should be designated. This limit would show whether this alloy contains ferromagnetic τ phase or the paramagnetic stable phases. This could be done by investigating a narrower range of composition such as 70 wt% Mn – 71.5 wt% Mn. Right now, it was observed that below the first limit the alloy could become ferromagnetic by forming τ phase, and above the second limit, it was paramagnetic and it contained β and γ_2 phases. Then, an alloy in the ferromagnetic range was investigated by in-situ HEXRD and it was observed that during the heating

of single ε phase alloy, first τ phase formation could be observed, then β phase formed and lastly γ_2 phase could be seen in the alloy. This was an important result that may be beneficial in obtaining single and more stable τ phase alloy which would provide much higher magnetic properties. This investigation was also helpful with kinetic analysis. The three peak fit procedure was applied to the DSC scans and the peak temperatures of all three phase formations were obtained. Therefore, Kissinger and Ozawa methods were applied and it was calculated that the activation energies of the phases τ, β, and γ_2 were; 140 kJ/mol, 168 kJ/mol, and 179 kJ/mol, respectively. The microstructural observation of τ phase was conducted. τ phase appears to be a plate-like feature under all of the microscopic techniques used.

In the second part, by the help of detailed in-situ HEXRD experiments, the cause of composition dependence of τ phase formation was found. With the help of synchrotron light, ε' phase was observed in the alloys which seems to cause τ phase formation in the alloys with lower manganese content. On the other hand, the distinctive ε' peak was not observed for higher manganese content which resulted in the formation of stable phases even the sample was initially containing single ε phase.

5.2 Future Recommendations

There is so much to learn about Mn-Al alloys. This study was an introduction to understanding this system by the help of high-energy XRD techniques. These should be supported by morphological analyses. Microscopy techniques, particularly TEM could give a lot of information about the system. There have been some studies with this aspect, but these should be conducted and related with the XRD and DSC analyses to further confirmation because there seems to be still some unclear parts. Moreover, the crystallographic analysis should be done in more detail with HEXRD, in-situ TEM, and EBSD techniques which would give more information about the orientation of the system and by different production techniques and with more information, the magnetic properties could be improved. With this kind of characterization techniques, all of the morphology and crystallography could be understood better. The relationship

between defects in the system and the phases forming could be solved. For instance, how the ε' phase is effected due to the defects in the system and why it is happening in samples with lower manganese content.

Moreover, since the addition of carbon is said to stabilize the τ phase, the addition of a third component should be further investigated. Rather than trial and error method, more detailed computational investigations can be done with this system. If these computational results and the experimental results are combined, the stabilization of τ phase and prevention of stable phase formation can be obtained which would lead to much higher magnetic properties and perhaps the conventional use of Mn-Al permanent magnets.

This study was also focused on isochronal studies. These samples should be investigated by isothermal studies, as well. The effect of kinetics, the time and temperature relationships should be resolved to obtain desired phase transformations and the maximum amount of τ phase without formation of the stable phases.

Since ε' phase has a crucial role in τ phase formation. Increasing this phase might be beneficial for improving the magnetic properties. Thus, the addition of carbon nanotubes may affect the phase transformation hierarchy and increase the amount of ε' phase, therefore, higher magnetic properties can be achieved.

REFERENCES

[1] H. W. Meyer, “A History of Electricity and Magnetism,” 1972.

[2] E. Du Tremolet de, D. Gignoux, and M. Schlenker, *Fundamentals of Magnetism*. Berlin, Heidelberg: Springer Berlin Heidelberg, 2006.

[3] W. D. Callister and D. G. Rethwisch, “Materials Science and Engineering: An Introduction, 8th Edition,” 2010.

[4] R. Skomski, P. Manchanda, P. K. Kumar, B. Balamurugan, A. Kashyap, and D. J. Sellmyer, “Predicting the Future of Permanent-Magnet Materials,” *IEEE Trans. Magn.*, vol. 49, no. 7, pp. 3215–3220, Jul. 2013.

[5] H. R. Kirchmayr, “Permanent magnets and hard magnetic materials,” *J. Phys. D. Appl. Phys.*, vol. 29, no. 11, pp. 2763–2778, Nov. 1996.

[6] R. Skomski and J. M. D. Coey, “Magnetic anisotropy — How much is enough for a permanent magnet?,” *Scr. Mater.*, vol. 112, pp. 3–8, Feb. 2016.

[7] F. Jimenez-Villacorta and L. H. Lewis, “Advanced Permanent Magnetic Materials,” *Nanomagnetism*, pp. 160–189, 2014.

[8] J. M. D. Coey, “Permanent magnetism,” *Solid State Commun.*, vol. 102, no. 2–3, pp. 101–105, Apr. 1997.

[9] J. M. D. Coey, “Permanent magnet applications,” *J. Magn. Magn. Mater.*, vol. 248, no. 3, pp. 441–456, Aug. 2002.

[10] E. A. Nesbitt and J. H. Wernick, “Rare Earth Permanent Magnets,” 1973.

[11] N. Vogel, *Rare Earth Elements A New Approach to the Nexus of Supply, Demand and Use: Exemplified along the Use of Neodymium in Permanent Magnets*. 2011.

[12] B. Bochenkov and S. Lutz, "A review of modern materials of permanent magnets," in *Proceedings. The 8th Russian-Korean International Symposium on Science and Technology, 2004. KORUS 2004.*, 2004, vol. 1, pp. 201–203.

[13] R. W. McCallum, L. Lewis, R. Skomski, M. J. Kramer, and I. E. Anderson, "Practical Aspects of Modern and Future Permanent Magnets," *Annu. Rev. Mater. Res.*, vol. 44, no. 1, pp. 451–477, Jul. 2014.

[14] J. J. Becker, "Permanent Magnets Based on Materials with High Crystal Anisotropy," *IEEE Trans. Magn.*, vol. MAG-4, no. 3, pp. 239–249, 1968.

[15] B. Slusarek and K. Zakrzewski, "Magnetic properties of permanent magnets for magnetic sensors working in wide range of temperature," *Prz. Elektrotechniczny*, vol. 88, no. 7, pp. 123–126, 2012.

[16] K. J. Strnat, "Modem Permanent Magnets for Applications in Electro-Technology," *Proc. IEEE*, vol. 78, no. 6, pp. 923–946, 1990.

[17] D. J. Sellmyer, B. Balamurugan, W. Y. Zhang, B. Das, R. Skomski, P. Kharel, and Y. Liu, "Advances in Rare-Earth-Free Permanent Magnets," pp. 7–14, 2013.

[18] S. Kozawa, "Trends and Problems in Research of Permanent Magnets for Motors — Addressing Scarcity Problem of Rare Earth Elements —," *Sci. Technol. Trends*, no. 38, pp. 40–54, 2011.

[19] A. Kallaste, T. Vaimann, and O. Pabut, "Slow-speed ring-shaped permanent magnet generator for wind applications Slow-Speed Ring-Shaped Permanent Magnet Generator for Wind Applications," *ResearchGate*, 2012.

[20] J. M. D. Coey, “New permanent magnets; manganese compounds,” *J. Phys. Condens. Matter*, vol. 26, pp. 1–6, Feb. 2014.

[21] C. Chinnasamy, M. M. Jasinski, A. Ulmer, W. Li, G. Hadjipanayis, and J. Liu, “Mn-Bi Magnetic Powders With High Coercivity and Magnetization at Room Temperature,” *IEEE Trans. Magn.*, vol. 48, no. 11, pp. 3641–3643, Nov. 2012.

[22] J. B. Yang, K. Kamaraju, W. B. Yelon, W. J. James, Q. Cai, and A. Bollero, “Magnetic properties of the MnBi intermetallic compound,” *Appl. Phys. Lett.*, vol. 79, no. 12, pp. 1846–1848, 2001.

[23] J. M. D. Coey, “Permanent magnets: Plugging the gap,” *Scr. Mater.*, vol. 67, no. 6, pp. 524–529, Sep. 2012.

[24] J. Winterlik, B. Balke, G. H. Fecher, C. Felser, M. C. M. Alves, F. Bernardi, and J. Morais, “Structural, electronic, and magnetic properties of tetragonal $Mn_{3-x}Ga$: Experiments and,” *Phys. Rev. B*, vol. 77, no. 5, p. 54406, Feb. 2008.

[25] J. W. Christian, *The Theory of Transformations in Metals and Alloys*, 3rd ed. Elsevier Science, 2002.

[26] D. A. Porter, K. E. Easterling, and M. Y. Sherif, *Phase Transformations in Metals and Alloys*, 3rd ed. 2009.

[27] J. L. H. Aaronson, M. Enomoto, *Mechanism of Diffusional Phase Transformations in Metals and Alloys*. 2010.

[28] G. Kostorz, *Phase Transformations in Materials*. 2001.

[29] H. E. Kissinger, “Reaction Kinetics in Differential Thermal Analysis,” *Anal. Chem.*, vol. 29, no. 11, pp. 1702–1706, 1957.

[30] T. Ozawa, “A New Method of Analyzing Thermogravimetric Data,” *Bull. Chem. Soc. Jpn.*, vol. 38, no. 11, pp. 1881–1886, 1965.

[31] K. Kamino, T. Kawaguchi, and M. Nagakura, “Magnetic Properties of MnAl System Alloys,” *IEEE Trans. Magn.*, vol. 2, no. 3, pp. 506–510, 1966.

[32] Y. Kurtulus and R. Dronskowski, “Electronic structure, chemical bonding, and spin polarization in ferromagnetic MnAl,” *J. Solid State Chem.*, vol. 176, no. 2, pp. 390–399, Dec. 2003.

[33] D. E. Laughlin, K. Srinivasan, M. Tanase, and L. Wang, “Crystallographic aspects of L10 magnetic materials,” in *Scripta Materialia*, 2005, vol. 53, no. 4, pp. 383–388.

[34] B. B. Lindahl and M. Selleby, “The Al-Fe-Mn system revisited-An updated thermodynamic description using the most recent binaries,” *Calphad Comput. Coupling Phase Diagrams Thermochem.*, vol. 43, pp. 86–93, 2013.

[35] R. Skomski, “Phase formation in L_10 magnets,” *J. Appl. Phys.*, vol. 101, no. 9, pp. 1–4, 2007.

[36] T. Klemmer, D. Hoydick, H. Okumura, B. Zhang, and W. A. Soffa, “Magnetic hardening and coercivity mechanisms in L_10 ordered FePd ferromagnets,” *Scr. Metall. Mater.*, vol. 33, no. 10–11, pp. 1793–1805, 1995.

[37] J. H. Park, Y. K. Hong, S. Bae, J. J. Lee, J. Jalli, G. S. Abo, N. Neveu, S. G. Kim, C. J. Choi, and J. G. Lee, “Saturation magnetization and crystalline anisotropy calculations for MnAl permanent magnet,” in *Journal of Applied Physics*, 2010, vol. 107, no. 9, p. 09A731.

[38] C. Yanar, J. M. K. Wiezorek, W. a Soffa, and V. Radmilovic, "Massive transformation and the formation of the ferromagnetic L_10 phase in manganese-aluminum-based alloys," *Metall. Mater. Trans. A*, vol. 33, no. 8, pp. 2413–2423, 2002.

[39] J. J. V. D. B. Broek and H. Donkersloot, "Phase Transformations in Pure and Carbon-Doped $Al_{45}Mn_{55}$ Alloys," *Acta Metall.*, vol. 27, pp. 1497–1504, 1979.

[40] T. Prost, "Magnetic Properties Study of the Mn-Al System with Additions of B or C and Mechanical Milling Techniques," *Eng. Mech. Diss. \& Theses*, p. 30, 2012.

[41] Q. Zeng, I. Baker, J. B. Cui, and Z. C. Yan, "Structural and magnetic properties of nanostructured Mn–Al–C magnetic materials," *J. Magn. Magn. Mater.*, vol. 308, no. 2, pp. 214–226, Jan. 2007.

[42] T. B. Massalski, *Binary Alloy Phase Diagrams*, vol. 2. 1990.

[43] J. Grosek and I. Baker, "Nanostructured Anisotropic Permanent Mn-Al and Mn-Al- C Magnets," pp. 1–5, 2007.

[44] H. X. Wang, "Structural Stabilizing Effect of Zn Substitution on MnAl and Its Magnetic Properties," *Open J. Microphys.*, vol. 1, no. 2, pp. 19–22, 2011.

[45] N. Singh, V. Mudgil, K. Anand, A. K. Srivastava, R. K. Kotnala, and A. Dhar, "Influence of processing on structure property correlations in τ-MnAl rare-earth free permanent magnet material," *J. Alloys Compd.*, vol. 633, pp. 401–407, 2015.

[46] J. M. Le Breton, J. Bran, E. Folcke, M. Lucis, R. Larde, M. Jean, and J. E. Shield, "Structural modifications in a $Mn_{54}Al_{43}C_3$ melt-spun alloy induced by mechanical milling and subsequent annealing investigated by atom probe tomography," *J. Alloys Compd.*, vol. 581, pp. 86–90, 2013.

[47] K. Kim and K. Sumiyama, “Ferromagnetic α-Mn-type Mn-Al alloys produced by mechanical alloying,” *J. Alloys Compd.*, vol. 217, pp. 48–51, 1995.

[48] J.-G. Lee, X.-L. Wang, Z.-D. Zhang, and C.-J. Choi, “Effect of mechanical milling and heat treatment on the structure and magnetic properties of gas atomized Mn–Al alloy powders,” *Thin Solid Films*, vol. 519, no. 23, pp. 8312–8316, Sep. 2011.

[49] Y. C. Yang, W. W. Ho, C. Lin, J. L. Yang, H. M. Zhou, J. X. Zhu, X. X. Zeng, B. S. Zhang, and L. Jin, “Neutron diffraction study of hard magnetic alloy MnAlC,” *J. Appl. Phys.*, vol. 55, no. 6, pp. 2053–2054, 1984.

[50] A. Chaturvedi, R. Yaqub, and I. Baker, “A comparison of τ-MnAl particulates produced via different routes,” *J. Phys. Condens. Matter*, vol. 26, no. 6, p. 64201, 2014.

[51] Q. Zeng, I. Baker, and Z. C. Yan, “Nanostructured Mn-Al permanent magnets produced by mechanical milling,” *J. Appl. Phys.*, vol. 99, no. 8, pp. 10–13, 2006.

[52] O. Obi, L. Burns, Y. Chen, T. Fitchorov, S. Kim, K. Hsu, D. Heiman, L. H. Lewis, and V. G. Harris, “Magnetic and structural properties of heat-treated high-moment mechanically alloyed MnAlC powders,” *J. Alloys Compd.*, vol. 582, pp. 598–602, Jan. 2014.

[53] P. C. Kuo, Y. D. Yao, W. R. Chen, and J. . Huang, “Preparation and magnetical studies of $Mn_{50}Al_{50}$/Al bilayer films,” *J. Appl. Phys.*, vol. 81, no. 8, pp. 5253–5255, 1997.

[54] W. Van Roy, H. Bender, C. Bruynseraede, J. De Boeck, and G. Borghs, “Degree of order and magnetic properties of , τ-MnAl films,” *J. Magn. Magn. Mater.*, vol. 148, pp. 97–98, 1995.

[55] G. A. Fischer and M. L. Rudee, “Effect of magnetic annealing on the τ-phase of MnAl thin films,” *J. Magn. Magn. Mater.*, vol. 213, no. 3, pp. 335–339, 2000.

[56] C. Y. Duan, X. P. Qiu, B. Ma, Z. Z. Zhang, and Q. Y. Jin, “The structural and magnetic properties of τ-MnAl films prepared by Mn/Al multilayers deposition plus annealing,” *Mater. Sci. Eng. B Solid-State Mater. Adv. Technol.*, vol. 162, no. 3, pp. 185–188, 2009.

[57] H. Fang, S. Kontos, J. Ångström, J. Cedervall, P. Svedlindh, K. Gunnarsson, and M. Sahlberg, “Directly obtained τ-phase MnAl, a high performance magnetic material for permanent magnets,” *J. Solid State Chem.*, 2016.

[58] L. G. Marshall, I. J. McDonald, and L. H. Lewis, “Quantification of the strain-induced promotion of τ-MnAl via cryogenic milling,” *J. Magn. Magn. Mater.*, vol. 404, pp. 215–220, 2016.

[59] A. Pasko, M. LoBue, E. Fazakas, L. K. Varga, and F. Mazaleyrat, “Spark plasma sintering of Mn-Al-C hard magnets,” *J. Phys. Condens. Matter*, vol. 26, no. 6, p. 64203, 2014.

[60] P. Saravanan, V. T. P. Vinod, M. Černík, A. Selvapriya, D. Chakravarty, and S. V. Kamat, “Processing of Mn-Al nanostructured magnets by spark plasma sintering and subsequent rapid thermal annealing,” *J. Magn. Magn. Mater.*, vol. 374, pp. 427–432, 2015.

[61] P. Blaha, K. Schwarz, P. Sorantin, and S. B. Trickey, “Full-potential, linearized augmented plane wave programs for crystalline systems,” *Comput. Phys. Commun.*, vol. 59, no. 2, pp. 399–415, 1990.

[62] K. Anand, J. J. Pulikkotil, and S. Auluck, “Study of ferromagnetic instability in τ-MnAl, using first-principles,” *J. Alloys Compd.*, vol. 601, pp. 234–237, 2014.

[63] P. Manchanda, A. Kashyap, J. E. Shield, L. H. Lewis, and R. Skomski,

"Magnetic properties of Fe-doped MnAl," *J. Magn. Magn. Mater.*, vol. 365, pp. 88–92, 2014.

[64] T. Saito, "Magnetic properties of Mn-Al system alloys produced by mechanical alloying," *J. Appl. Phys.*, vol. 93, no. 10 3, pp. 8686–8688, 2003.

[65] T. Saito, "Magnetic properties of Mn-Al-C alloy powders produced by mechanical grinding," *J. Appl. Phys.*, vol. 97, no. 10, 2005.

[66] F. Bittner, L. Schultz, and T. G. Woodcock, "Twin-like defects in $L_1$0 ordered τ-MnAl-C studied by EBSD," *Acta Mater.*, vol. 101, pp. 48–54, 2015.

[67] B. Foreback and I. Baker, "Permanent Magnets from Mechanically Milled $Mn_{54}Al_{46}$ Alloys," 2008.

[68] Q. Zeng, I. Baker, and Z. Yan, "Nanostructured Mn–Al permanent magnets produced by mechanical milling," *J. Appl. Phys.*, vol. 99, no. 8, p. 08E902, 2006.

[69] F. Jiménez-Villacorta, J. Marion, J. Oldham, M. Daniil, M. Willard, and L. Lewis, "Magnetism-Structure Correlations during the ε→τ Transformation in Rapidly-Solidified MnAl Nanostructured Alloys," *Metals (Basel).*, vol. 4, no. 1, pp. 8–19, 2014.

[70] T. Ohtani, N. Kato, S. Kojima, K. Kojima, Y. Sakamoto, I. Konno, M. Tsukahara, and T. Kubo, "Magnetic properties of Mn-Al-C permanent magnet alloys," *IEEE Trans. Magn.*, vol. 13, no. 5, pp. 1328–1330, 1977.

[71] J. Van Landuyt, G. Van Tendeloo, J. J. Van Den Broek, and H. Donkersloot, "Permanent magnetism and microstructure in τ-AlMn(C)," *J. Magn. Magn. Mater.*, vol. 15–18, no. PART 3, pp. 1451–1452, 1980.

[72] Y. J. Kim and J. H. Perepezko, “The thermodynamics and competitive kinetics of metastable τ phase development in MnAl-base alloys,” *Mater. Sci. Eng. A*, vol. 163, no. 1, pp. 127–134, 1993.

[73] D. C. Crew, P. G. McCormick, and R. Street, “MnAl and MnAlC permanent magnets produced by mechanical alloying,” *Scr. Metall. Mater.*, vol. 32, no. 3, pp. 315–318, 1995.

[74] P. Muellner, B. E. Buergler, H. Heinrich, A. S. Sologubenko, and G. Kostorz, “Observation of the shear mode of the ε→τ phase transformation in a Mn-Al-C single crystal,” *Philos. Mag. Lett.*, vol. 82, no. 2, pp. 71–79, 2002.

[75] D. P. Hoydick, E. J. Palmiere, and W. A. Soffa, “On the Formation of The Metastable $L_1$0 Phase in Manganese-Aluminum-Base Permanent Magnet Materials,” *Scr. Mater.*, vol. 36, no. 2, pp. 151–156, 1997.

[76] D. P. Hoydick, E. J. Palmiere, and W. a. Soffa, “Microstructural development in MnAl-base permanent magnet materials: New perspectives,” *J. Appl. Phys.*, vol. 81, no. 8, p. 5624, 1997.

[77] C. Yanar, V. Radmilovic, W. A. Soffa, and J. M. K. Wiezorek, “Evolution of microstructure and defect structure in $L_1$0-ordered manganese aluminide permanent magnet alloys,” *Intermetallics*, vol. 9, pp. 949–954, 2001.

[78] J. M. K. Wiezorek, A. K. Kulovits, C. Yanar, and W. A. Soffa, “Grain boundary mediated displacive-diffusional formation of τ-phase MnAl,” *Metall. Mater. Trans. A Phys. Metall. Mater. Sci.*, vol. 42, no. 3, pp. 594–604, 2011.

[79] Y. Sakka, M. Nakamura, and K. Hoshimoto, “Rapid quenching and properties of hard magnetic materials in MnAl-X (X = Ti, Cu, Ni, C, B) systems,” *J. Mater. Sci.*, vol. 24, pp. 4331–4338, 1989.

[80] Z. W. Liu, C. Chen, Z. G. Zheng, B. H. Tan, and R. V. Ramanujan, “Phase

transitions and hard magnetic properties for rapidly solidified MnAl alloys doped with C, B, and rare earth elements," *J. Mater. Sci.*, vol. 47, no. 5, pp. 2333–2338, Oct. 2012.

[81] J. J. Wysłocki, P. Pawlik, and A. Przybył, "Magnetic properties of the non-oriented τ-phase in Mn-Al-C permanent magnet," *Mater. Chem. Phys.*, vol. 60, no. 2, pp. 211–213, 1999.

[82] E. Fazakas, L. K. Varga, and F. Mazaleyrat, "Preparation of nanocrystalline Mn–Al–C magnets by melt spinning and subsequent heat treatments," *J. Alloys Compd.*, vol. 434–435, pp. 611–613, May 2007.

[83] O. Kohmoto, N. Kageyama, Y. Kageyama, H. Haji, M. Uchida, and Y. Matsushima, "Magnetic properties of mechanically alloyed Mn-Al-C powders," *J. Phys. Conf. Ser.*, vol. 266, p. 12016, Jan. 2011.

[84] V. 2 ASM International Handbook, "Properties and selection: Nonferrous alloys and special-purpose materials," *ASM Met. Handb.*, vol. 2, p. 1300, 1990.

[85] A. S. Sologubenko, P. Müllner, H. Heinrich, M. Woligarten, and G. Kostorz, "The effect of composition and stress on the selection of ε→τ transformation modes in MnAl-C," *J. Phys. IV*, vol. 112, pp. 1071–1074, Oct. 2003.

[86] M. A. Uimin, A. E. Ermakov, O. B. Andreeva, E. I. Teitel, and V. M. Gundyrev, "Phase transformations and magnetic properties of MnAl-C single crystals," *Phys. status solidi*, vol. 88, no. 2, pp. 587–594, Apr. 1985.

[87] V. M. Gundyrev, M. A. Uimin, A. E. Ermakov, and O. B. Andreeva, "Transformation in MnAl-C Alloys," *Phys. status solidi*, vol. 91, no. 1, pp. K55–K58, Sep. 1985.